

A Personalized Fluid-structure Interaction Modeling Paradigm for Aorta in Human Fetuses

Zhenglun Alan Wei^{1,*}, PhD; Guihong Chen^{2,*}, MD; Biao Si¹, MD, PhD; Liqun Sun³, MD PhD; Mike Seed³, MD; and Shuping Ge⁴, MD

¹Department of Biomedical Engineering, Worcester Polytechnic Institute, Worcester, MA, USA

²Medical Ultrasound Department, The Fourth Hospital of Shijiazhuang, Shijiazhuang, China

³Division of Cardiology, Department of Pediatrics, The Hospital for Sick Children, University of Toronto, Toronto, Canada

⁴Department of Pediatric and Adult Congenital Cardiology, Geisinger Heart and Vascular Institute, Geisinger Clinic, Danville, PA, USA

* This work is a result of the equal contributions of the following authors.

Please send the correspondence of the current work to

Name: Zhenglun Alan Wei, PhD

Address: 60 Prescott Street

Phone: 978-934-3754

Fax:

E-mail: ZWei1@wpi.edu

Name: Shuping Ge, MD, FACC, FAHA, FASE

Address: 100 N. Academy Avenue, Danville, PA 17822

Phone: 570-271-6466

Fax: 570-214-1480

E-mail: sge@geisinger.edu

Word Count: 5966 (Limit: N/A)

Keywords

Fluid-structure interaction; Computational fluid dynamics; medical image processing; fetal circulation;

Personalized physiological modeling

Abstract (Word Count: 232; Limit: 250)

Fluid-structure interaction (FSI) modeling, a technique widely used to enhance imaging modalities for adult and pediatric heart diseases, has been *underutilized in the context of fetal circulation because of limited data* on flow conditions and material properties. Recognizing the significant impact of congenital heart diseases on the fetal aorta, our research aims to address this gap by developing and validating a personalized FSI model for the fetal aorta.

Our approach involved reconstructing the anatomy and flow of the fetal aorta using fetal echocardiography and ultrasound. We developed an innovative iterative method that includes: (i) an automated process for incorporating Windkessel models at outflow boundaries when clinical data is limited because of the resolution constraints of fetal imaging, (ii) an inverse approach to estimate bulk material properties, and (iii) an FSI model for high-fidelity hemodynamic evaluation. This method is efficient, typically converging in fewer than three iterations.

We analyzed four normal fetal aortas with gestational ages ranging from 23.5 to 35.5 weeks to validate our workflow. We compared results with *in vivo* velocity waveforms across a cardiac cycle at the aortic isthmus. Strong correlations ($R > 0.95$) were observed. Furthermore, our findings suggest that the stiffness of the fetal aorta increases until 30 weeks of gestation and then decreases.

This study marks a *first-of-its-kind* effort in developing a rigorously validated, personalized flow model for fetal circulation, offering novel insights into fetal aortic development and growth.

ABBREVIATIONS

2D	two-dimensional
3D	three-dimensional
AAo	ascending aorta
AoA	aortic arch
PA	pulmonary artery
ThAo	thoracic aorta.
AoI	aortic isthmus
BA	brachiocephalic artery
CHD	congenital heart disease
DA	ductus arteriosus
DAo	descending aorta
FE	fetal echocardiography
FEA	finite element analysis
FSI	fluid-structure interaction
GA	gestational age
LCCA	left common carotid artery
LSA	left subclavian artery
PyAuto3WK	in-house Python code
R	distal resistance
WK	Windkessel
WSS	wall shear stress
Z	proximal resistance

A. Introduction

Congenital heart disease (CHD) is the most common congenital disability and a leading cause of death and chronic disease in newborns, infants, and children [1-3]. Prenatal screening and identification of CHD provide the earliest window of opportunity to improve the understanding of its pathogenesis, timely diagnosis/prognosis, parental counseling, safety, and effective therapy for optimal perinatal and long-term outcomes [4, 5]. However, there are numerous challenges in clinical care and innovation in CHD due to the lack of animal models, its rarity, and limited resolutions of contemporary fetal imaging methods for the accurate prenatal diagnosis and prognosis of CHD [6, 7].

Computational flow modeling has been used to augment medical imaging modalities and capture high-fidelity hemodynamics in the cardiovascular system in a personalized fashion. Many previous studies have used computational models to understand and uncover the mechanism, improve diagnosis/prognosis, and develop treatment methods such as medical devices and therapies for adult and pediatric heart diseases [8-11]. However, data for developing a computational model for fetal circulation are scarce. *Few models have been rigorously validated* against clinical measurements. Wiputra *et al.* developed a computational model to simulate the fetal right ventricle and obtained “generally good agreements” between their simulated data and a range of published data [12]. Later, the same group presented a plausible study to validate their model against clinically measured velocity by echocardiography. However, their validation focused on the velocity at specific time points of a cardiac cycle such as, at peak systole, instead of time-resolved quantities over the whole cardiac cycle [13]. Last year, Salman *et al.* used the model from Wiputra’s study and confirmed that the model produces results that qualitatively agree with the data found in the literature [14].

The fetal aorta is involved in many CHDs, such as coarctation of the aorta (CoA), patent ductus arteriosus (DA), and transposition of the great arteries. Researchers have developed many computational models for the aorta in pediatric or adult patients [15-20]. However, the fetal aorta is NOT a smaller version of the pediatric or the adult aorta; both of which have an additional vessel (the DA) (Figure 1) that makes the anatomy and flow conditions more complex.

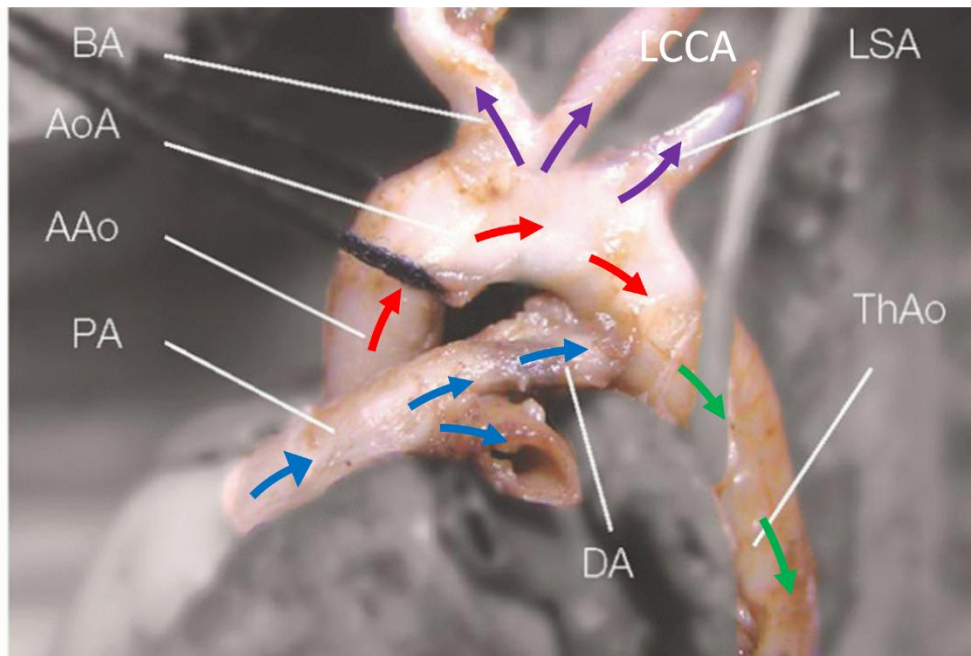


Figure 1. An illustration of the fetal aorta in a healthy individual [21]. AAo: ascending aorta; AoA: aortic arch; BA: brachiocephalic artery; DA: ductus arteriosus; LCCA: left common carotid artery; LSA: left subclavian artery; PA: pulmonary artery; and ThAo: thoracic aorta.

Previous studies used zero-dimensional lumped parameter models that simulate the hemodynamics in the fetal aorta using a simplified relation between flow rate and pressure drop [22-25]. Recent studies used computational fluid dynamics models to capture high-fidelity three-dimensional (3D) hemodynamics for the fetal aorta [26-28]. However, these models overlook many essential patient characteristics such as, the material properties of the vessel, which could lead to significant errors in calculating hemodynamic metrics [15, 19, 20, 29]. More importantly, these models have yet to be validated. Therefore, to date, there is *no rigorously validated computational model* for the fetal aorta.

Thus, this study aimed to develop a novel, personalized flow model to assess the hemodynamics of the fetal aorta and validate it using *in vivo* measurements. The developed model involves personalized anatomy, flow, and material properties of the fetal aorta. The validated model can be used to understand the pathogenesis of CHD related to the fetal aorta, improve pertinent diagnostic/prognostic methods, and investigate the feasibility, safety, and efficacy of therapeutic strategies.

B. Materials and Methods

The process of developing the fluid-structure interaction (FSI) model begins with the anatomical reconstruction of the fetal aorta, utilizing images and data obtained from dynamic 3D SpatioTemporal Image Correlation fetal

echocardiography (FE), as depicted in Figure 2a (further details in Section B.2). In parallel, time-varying flow rates were calculated based on blood flow velocity data acquired using spectral Doppler methods (Figure 2b; details in Section B.3). The anatomy and flow were thoroughly discussed and validated by the clinical contributors to this study (GC, LS, MS), with final verification by GS, before incorporating them into the novel iterative process shown in Figure 2c. This process involves finite element analysis (FEA) and an in-house Python code to estimate material properties and Windkessel (WK) parameters of the fetal aorta. This combined approach culminated in an FSI model that enabled personalized assessment of fetal aortic hemodynamics.

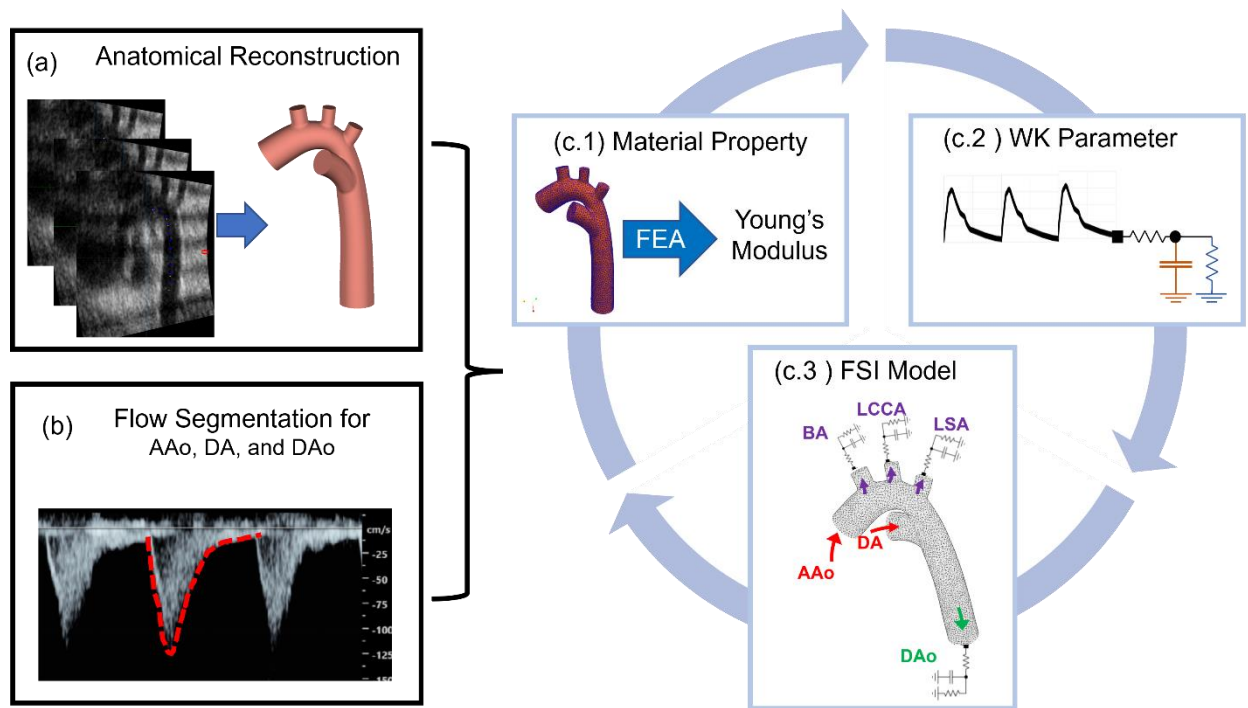


Figure 2. Proposed modeling pipeline for the fluid-structure interaction model. (a) The general steps used in this study start with anatomical reconstruction. Meanwhile, flow segmentation for the aortic arch, ductus arteriosus, and descending aorta is conducted, as shown in (b). (c) A sketch of the iterative approach proposed in this study that involves (c.1), a finite element analysis to estimate the bulk material property of the fetal aorta; (c.2) a Python code to tune automatically for parameters of the model, and (c.3), a fluid-structure interaction that reflects physiologically realistic pressure and flow inside the fetal aorta. AAo: ascending aorta; AoA: aortic arch; BA: brachiocephalic artery; DA: ductus arteriosus; DAo: descending aorta; FSI: fluid-structure interaction; LCCA: left common carotid artery; LSA: left subclavian artery; PA: pulmonary artery; WK: Windkessel.

B.1 Study Subjects

The patients included in this study were retrospectively selected with the following criteria:

- Inclusion criteria: (i) Singleton pregnancy; (ii) gestational age (GA) > 20 weeks and < 40 weeks; (iii) no structural defect, heart failure, or arrhythmia in the fetus.

- Exclusion criteria: (i) Cardiac condition [e.g., fetal cardiac dysfunction and/or fetal hydrops, fetal arrhythmia, abnormal baseline heart rate (<110 bpm or > 160 bpm)]; (ii) multiple pregnancies, and (iii) fetal growth restriction (<3rd centile).

Standard ultrasound systems (GE Voluson E-10) were used to acquire two-dimensional (2D), 3D, and Doppler FE. The long-axis acquisition was used to capture the center plane of the aortic arch with the ascending aorta (AAo), aortic arch, the descending aorta (DAo), the brachiocephalic artery (BA), the left common carotid artery (LCCA), and the left subclavian artery (LSA). The short-axis acquisition should exhibit the center plane of the 3-vessel view, including the aortic and ductal arch structures. The 2D FE images were also acquired. Doppler velocity tracing was recorded for the AAo, DA, aortic isthmus (AoI), and DAo. There was no clinical measurement in the LCCA, the LSA, and the BA, primarily because of small vessel sizes and challenges in designating an appropriate field of view.

B.2 Anatomy Reconstruction and Flow Segmentation

Three-dimensional FE acquisition generally includes approximately 30 slices spatially (with 0.5 mm thickness) and 7–13 time frames. The frame of the smallest volume of the fetal aorta (during end-diastole) was chosen for anatomical reconstruction using SimVascular [30]. First, the center plane of the fetal aorta was identified, highlighting the center plane of the aortic arch and its bifurcations to the LCCA, LSA, and BA. The next step was determining the bifurcation between the aortic arch and the DA after the centerlines of the aortic arch; the LCCA, LSA, BA, and DA were identified and then lofted, assuming their structures to be circular cylinders. The diameter of the lofted vessels was compared with the clinical measurements done in 2D FE, which is the current gold standard. All 2D FE measurements were verified by SG (the last author), who has over 20 years of clinical experience in acquiring and analyzing FE images and data.

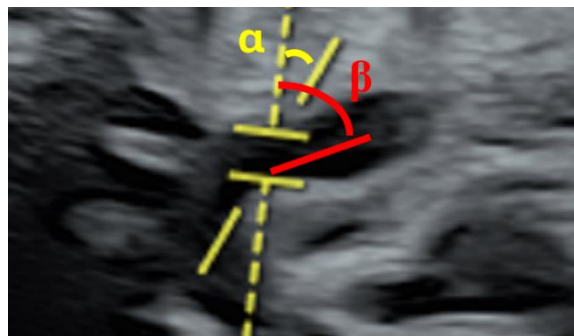


Figure 3 Angle correction of the velocity tracking

Doppler data were digitized and denoted as $V_{segmented}$. The ultrasound machine applied an initial angle correction (α) to the velocity tracking, as shown in Figure 3. However, this angle may differ from the actual angle (β) between the ultrasound beam and the true centerline of the vessel. This discrepancy primarily arises because of limitations in anatomical resolution when imaging fetal circulation [31, 32]. If the angle discrepancy ($\beta - \alpha$) exceeded 20 degrees (introducing about a 10% error [33]), a secondary angle correction was applied to the velocity waveforms using the formula, $V_{corrected} = V_{segmented} \times (\cos\alpha / \cos\beta)$, consistent with the initial angle correction implemented by the ultrasound machine [31, 33]. The vessel flow rate (Q) was then calculated using the corrected velocity and vessel diameter: $Q = \pi r^2 V_{corrected}$, where r is the radius of the vessel.

B.3 Estimation of Material Property

The bulk material property of a fetal aorta was estimated using a similar inverse method with an FEA [34, 35]. The process started with an initial guess of Young's modulus. A pulse pressure (ΔP) was applied inside the reconstructed fetal aorta (at its smallest volume). The vessel inflation function of SimVascular was used to deform the fetal aorta based on the current value of Young's modulus [36]. The vessel diameters of AoI in the deformed state were compared against clinical measurements. If the discrepancies were found to have exceeded 5%, Young's modulus was adjusted following the Newton-Raphson method, and another FEA based on the updated modulus was conducted. We adopted three assumptions commonly accepted by previous studies: (i) a homogeneous, linear elastic material model [19, 37]; (ii) the vessel wall thickness as 15% of the average radius of all vessel ends associated with the fetal aorta [25, 38]; and (iii) the Poisson ratio as 0.499 [37-39]. The challenge of deriving physiologically realistic material properties lies in selecting the appropriate pulse pressure to construct the traction vector, as detailed in Section B.6, which describes the iterative process.

B.4 Fluid-Structure Interaction Modeling

SimVascular has been used to generate the computational mesh, and the coupled momentum method has been used to conduct the FSI simulations [40]. In this method, a linearized kinematics Eulerian approach is adopted for monolithically coupling the fluid and solid domains. The fluid-solid meshes are kept fixed; therefore, the degrees of freedom of the vessel wall and the fluid boundary are identical, thus naturally satisfying the no-slip condition.

The incompressible Navier-Stokes equations were solved in the fluid domain:

$$\nabla \cdot \mathbf{v} = 0, \quad \rho \mathbf{v}_{,t} + \rho \mathbf{v} \cdot \nabla \mathbf{v} = -\nabla p + \nabla \cdot \boldsymbol{\tau} \quad (1)$$

where \mathbf{v} represents the blood velocity vector, ρ is the density of blood, p stands for pressure, and $\boldsymbol{\tau}$ is the viscous stress tensor defined as $\boldsymbol{\tau} = \mu(\nabla \mathbf{v} + (\nabla \mathbf{v})^T)$.

The vessel wall mechanics are approximated using a thin-walled structure assumption. Therefore, the solid domain is topologically defined by the same surface as the lateral boundary of the fluid domain. The elastodynamic equations, including boundary and initial conditions, for the vessel wall can be expressed as follows.

$$\rho^s \mathbf{u}_{,tt} = \nabla \cdot \boldsymbol{\sigma}^s + \mathbf{b}^s \quad (2)$$

where \mathbf{b}^s is a body force per unit volume, and $\boldsymbol{\sigma}^s(\mathbf{u})$ is the vessel wall Cauchy stress tensor.

In FSI simulations for cardiovascular modeling, Neumann boundary conditions (typically applied at outlets) may experience backflow because of either complete flow reversal (resulting from conservation of mass) or partial reversal caused by vortical structures near the boundary. This issue is particularly common when using the Windkessel model at the boundary [41-43]. Backflow can contribute to the numerical divergence of the simulation; therefore, backflow stabilization techniques are often implemented to mitigate this problem. In this study, we adopted the default backflow stabilization method provided by SimVascular, which introduces an additional convective term to the Neumann boundary condition [43]. Previous studies have shown that this stabilization technique offers a more robust and effective solution for handling flow reversals at Neumann boundaries compared to alternative methods, such as using Lagrange multipliers or constraining the velocity to be normal to the outlet [30, 44].

Inspired by Womersley's deformable wall theory, the coupled momentum method adopts a condition between the fluid and the solid domains: surface traction equality. The surface traction t^f acting on the fluid lateral boundary because interaction with the solid is equal and opposed to the surface traction t^s acting on the vessel wall due to the fluid: $t^f = -t^s$. Using a thin-wall approximation, the surface traction t^s can be used to define a fictitious body force \mathbf{b}^s acting on the solid domain. Thus, on Γ_s we have: $\mathbf{b}^s = -t^f/h$, where h is the thickness of the vessel wall.

The linear solver employed was the generalized minimal residual method (GMRES), with a modified Newton-Raphson method applied for linearization. The convergence threshold for fluid-solid interaction was set at 10^{-6} . The time-step size was determined as $T/800$, where T represents the duration of the cardiac cycle. No turbulence

modeling was involved because the Reynolds numbers based on the DAo for the subjects were 548 ± 200 . Blood was treated as a single-phase, Newtonian fluid using the previously published relation for fetal aortas [25]:

$$\mu = (1.15 + 0.075 \times GA)/1000 \text{ (kg/m-s)} \quad (3)$$

A periodically stable solution is often achieved after the simulation completes two cardiac cycles. However, all cases were run for five cycles, and the data from the ending cycle were post-processed for reporting.

B.5 Boundary Conditions

Womersley velocity profiles were applied to the AAO and DA along with imposing 3-element WK models on BA, LCCA, and LSA, and DAo, as shown in Figure 4.

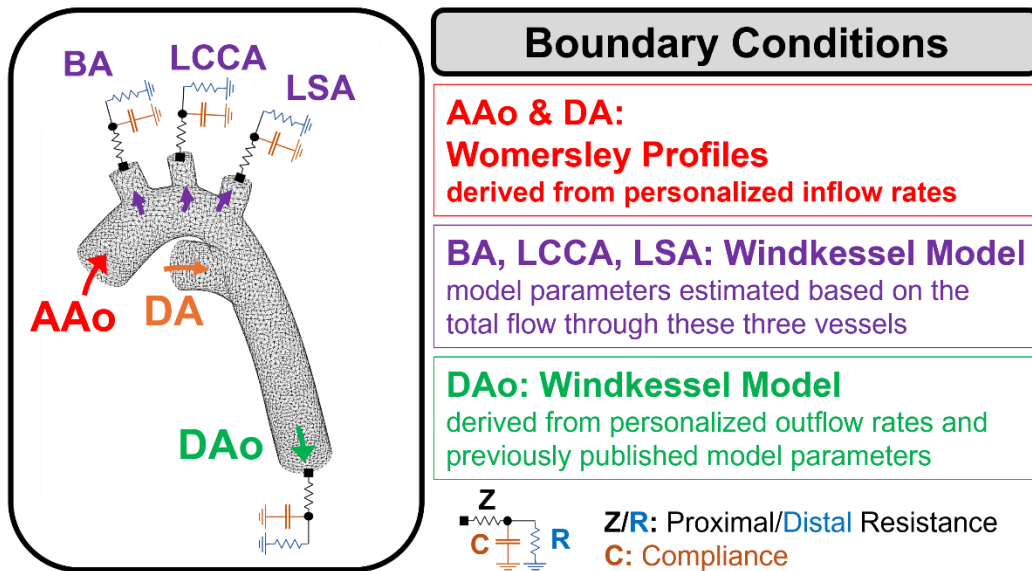


Figure 4. The mesh and boundary conditions of the final fluid-structure interaction model. AAO: ascending aorta; BA: brachiocephalic artery; DA: ductus arteriosus; DAo: descending aorta; LCCA: left common carotid artery; LSA: left subclavian artery.

An in-house Python code, PyAuto3WK, was developed to automate the estimation of parameters for the WK model. This code takes the *in vivo* flow measurement as input and generates the proximal and distal resistance (Z and R, respectively) and compliance as outputs. Pattern search optimization is employed to automatically seek the values of Z, R, and compliance (C) that reconcile the output pressures with the target mean and pulse pressure while ensuring that proximal resistance remains below 10% of the distal resistance ($Z < 0.1R$). This constraint between Z and R reflects a physiological state validated by clinical measurements [45] and is widely accepted in numerical studies [36, 46-49].

B.5.1 Windkessel Parameters for the Descending Aorta

Obtaining the WK parameters for the DAo is relatively simple. The input flow is acquired through in vivo Doppler measurements. Because invasive pressure measurements are unavailable, we relied on previously documented mean and pulse pressure values for the DAo in fetuses, which depend on GA [25, 39]. These values are denoted as $\overline{P_{DAo_GA}}$ and ΔP_{DAo_GA} , respectively.

$$\overline{P_{DAo_GA}}(mmHg) = 0.87 \times GA + 10.33 \quad (4)$$

$$\Delta P_{DAo_GA}(mmHg) = 0.39 \times GA + 13.44 \quad (5)$$

B.5.2 Windkessel Parameters for the Three Branches

Estimating the WK parameters for the BA, LCCA, and LSA (hereafter referred to as the “three branches”) presents three main challenges:

1. *Lack of in vivo flow measurements for the BA, LCCA, and LSA.* To address this issue, we estimate their total flow rate using $Q_{3b} = Q_{AAo} + Q_{DA} - Q_{DAo}$.
2. *Absence of in vivo pressure measurements or reported literature values for the three branches.* Consequently, we initially used literature-reported pressures at the DAo as a starting point [equations (4) and (5)]. Subsequently, we refined the pressure estimation at the three branches through an iterative process proposed in this study (details provided in Section B.6).
3. *No validated method for “splitting” the WK parameters for the BA, LCCA, and LSA in the fetal aorta.* Upon calculating the total WK parameters for the three branches, we need to “split” them accordingly to the BA, LCCA, and LSA.
 - a. The “splitting” algorithm for the total resistance (R_{total}) was usually based on the radius of the branches:

$$R_i = R_{total} \frac{\sum r_i^m}{r_i^m} \quad (6)$$

where R_i and r_i ($i = 1, 2, 3$) are the resistance and radius of the three branches, respectively. The coefficient m in the power law varies based on different theories. The “square law” ($m = 2$) is derived from curve-fitting clinical data in various scenarios, such as the internal carotid artery [50] and the major branches of the adult aorta [51]. The “cube law” ($m = 3$) adheres to Murray’s law,

which dictates the physiological principle of minimum work [52, 53]. The “fourth-order law” follows the Hagen-Poiseuille law, where flow resistance is proportional to the square of the vessel area. This law has been applied in the 0D hemodynamic assessment of the fetal aorta [25].

- b. The total compliance (C_{total}) has a similar “splitting” algorithm:

$$C_i = C_{total} \frac{r_i^m}{\sum r_i^m} \quad (7)$$

where C_i ($i = 1, 2, 3$) is the compliance of the three branches. The “square law” ($m = 2$) has been used for the adult aorta [33], and the “cube law” ($m = 3$) has been used in 0D flow modeling of the fetal aorta [24].

No prior studies have addressed the optimal power law for the 3D hemodynamic assessment of the three branches of the fetal aorta. Consequently, this study investigates and compares the effectiveness of these laws for this purpose.

B.6 Iterative Process

The goal of this iterative procedure is to achieve physiologically reasonable pressure within the fetal aorta. Once again, the pressure drop attributed to the inclusion of the DA flow (as explained in the Introduction) renders it impractical to rely on $\overline{P_{DAo_GA}}$ and ΔP_{DAo_GA} for obtaining physiologically reasonable material properties (described in Section B.2) and WK parameters for the three branches (described in Section B.5).

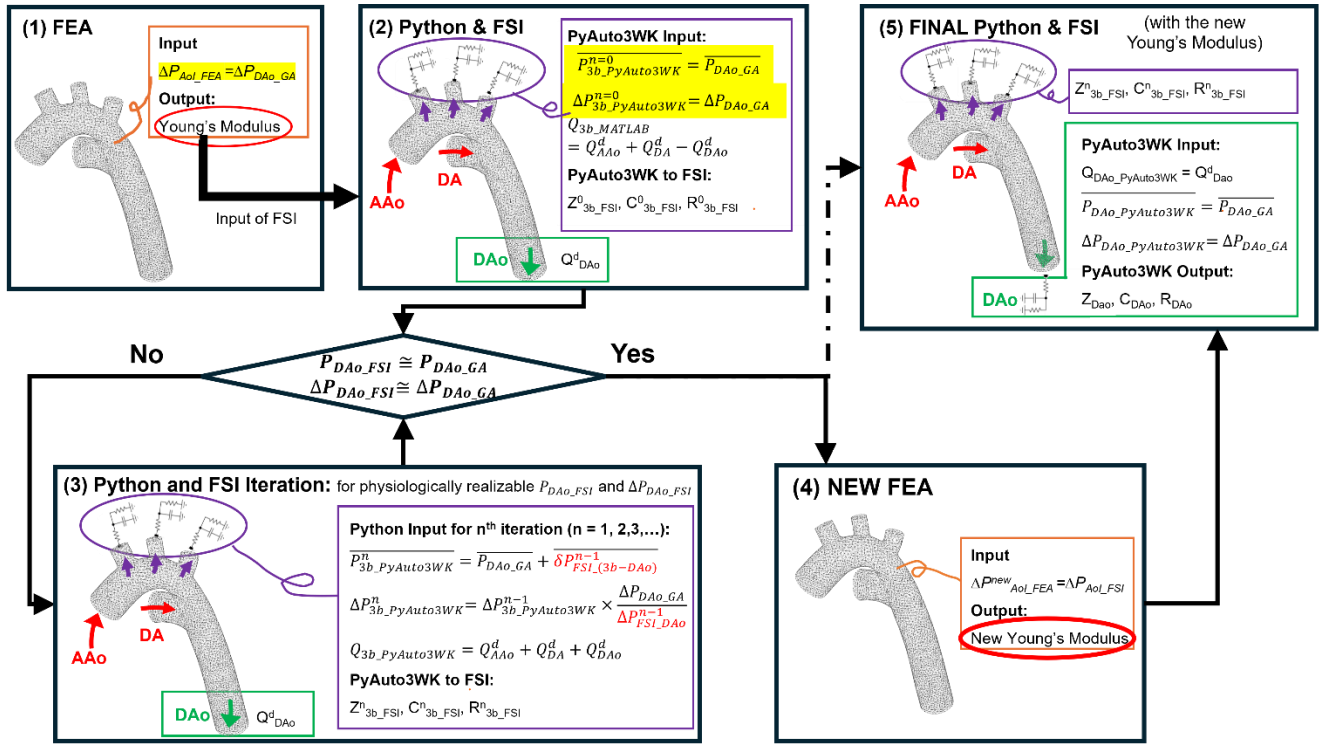


Figure 5. Workflow of the iterative process proposed in this study. In steps 1 and 2, the highlighted equations utilize pressure data from the literature for the descending aorta as an initial approximation for the pressures at the aortic isthmus and the three branches. Although this initial approximation is not physiologically accurate, it serves as a starting point for the subsequent steps. AAo: ascending aorta; AoI: aortic isthmus; C: compliance; DA: ductus arteriosus; DAo: descending aorta; FEA: finite element analysis; FSI: fluid-structure interaction; GA: gestational age; PyAuto3WK: in-house Python code; R: distal resistance; Z: proximal resistance.

Therefore, we devised an iterative process comprising five steps, delineated in Figure 5. These steps can be divided into three stages:

- *The initial stage* encompasses steps 1 and 2 depicted in Figure 5. During this step, we initially employed ΔP_{DAo_GA} as the first guess of pulse pressure at the AoI for the FEA (ΔP_{AoI_FEA} in Figure 5) to approximate a bulk material property of the fetal aorta. In step 2, we utilized the pressure at DAo from the literature [ΔP_{DAo_GA} and $\overline{P_{DAo_GA}}$, equation (4) and (5)] in the PyAuto3WK code to estimate the WK parameter for the three branches. It is noteworthy that, in this step, the FSI setup differs slightly from the one illustrated in Figure 4. The only difference lies in the boundary condition at the DAo, which is an outflow velocity condition based on the *in vivo* measurement rather than on a WK model.
- *The iterative stage* comprises step 3 in Figure 5, which involves multiple iterations between the FSI model and the PyAuto3WK code. For each iteration n :

- The simulated pressures at DAo ($\overline{P_{DAo_FSI}}$ and ΔP_{DAo_FSI}) and at the three branches $\overline{P_{3b_FSI}}$ were first obtained from the FSI model of iteration $n-1$.
 - $\overline{P_{DAo_FSI}}$ was used to calculate the pressure drop from the three branches to DAo: $\overline{\delta P_{FSI_{(3b-DAo)}}} = \overline{P_{FSI_{3b}}} - \overline{P_{FSI_{DAo}}}$, which was then used to update the mean pressure of the three branches in our PyAuto3WK code.
 - ΔP_{DAo_FSI} corrected the pulse pressure of the three branches in the PyAuto3WK code.
- The iteration ceased when the stimulated mean and pulse pressure at DAo agreed well with the literature data (within a 5% of error margin).
- *The final correction stage* includes steps 4 and 5 in Figure 5. By the conclusion of step 3, the pressures at the three branches and AoI could be remarkably different from their initial value used in *the initial stage* (steps 1 and 2). Consequently, it is appropriate to use the updated ΔP_{AoI_FSI} , which is more physiologically acceptable than ΔP_{DAo_GA} , to re-estimate the bulk material property of the fetal aorta. Employing this updated material property and the last set of WK parameters for the three branches from step 3, another FSI model is constructed in step 5. This FSI mirrors the one illustrated in Figure 4, where the DAo also uses a WK model, whose parameters were directly calculated from the PyAuto3WK code based on *in vivo* measured DAo flow and pressures at DAo from the literature [equations (4) and (5)].

B.7 Statistical Analysis

The primary outputs of the FSI model include velocity, pressure, and wall shear stress (WSS). Statistical analyzes were performed using IBM SPSS Statistics (IBM, Inc., Aramark, NY, USA). The metrics were first analyzed for normality using the Shapiro-Wilk test. Depending on normality results, either a Pearson or a Spearman correlation test was employed to ascertain the correlation between the FSI-derived metrics and the *in vivo* measurements.

C. Results

C.1 Patient Selection

The personalized anatomies for all subjects have been successfully reconstructed, as shown in Figure 6. All anatomies were plotted on the same dimensional scale to facilitate the visualization of their size differences.

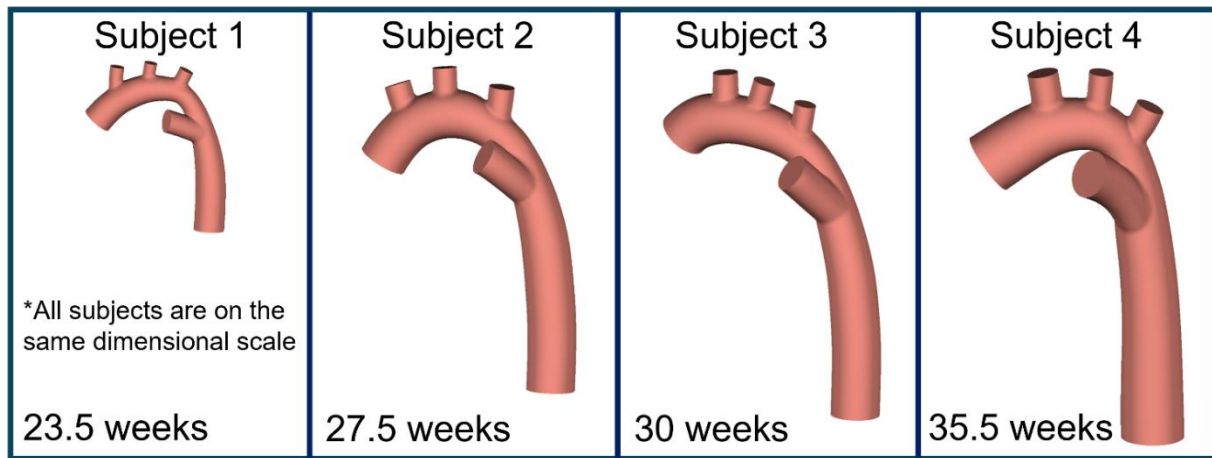


Figure 6. Personalized anatomies for all subjects, with the corresponding gestational age.

These individuals cover the typical GA range that was feasible for FE acquisition. In Figure 7, the vessel size determined by 2D FE and FSI was also compared, and good agreements were obtained. Table 1 shows the flow information of AAO, DA, and DAo. All vessels presented an increasing flow rate with GA. The highest Reynolds numbers in each subject occur at DAo; none exceeds the critical Reynolds number for a circular tube, i.e., 2000.

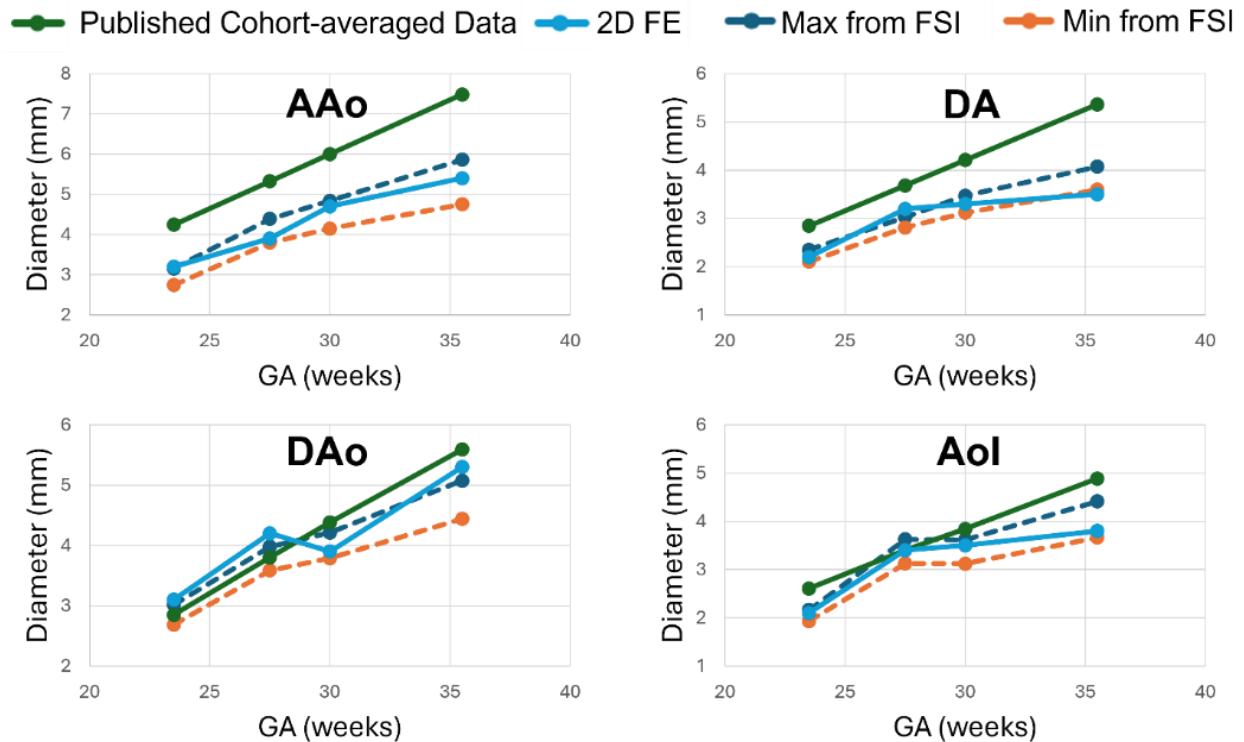


Figure 7. Comparisons of vessel sizes between two-dimensional fetal echocardiography, fluid-structure interaction, and published cohort-averaged data [25]. 2D: two-dimensional; AAO: ascending aorta; AoI: aortic isthmus; DA: ductus arteriosus; DAo: descending aorta; FE: fetal echocardiography; FSI: fluid-structure interaction; GA: gestational age.

Table 1. Summary of flow rate and Reynolds number for ascending aorta, ductus arteriosus, and descending aorta.

	AAo		DA		DAo	
	Q (mL/min)	Re	Q (mL/min)	Re	Q (mL/min)	Re
Subject 1 (23.5 weeks)	134	310	57.4	185	112	268
Subject 2 (27.5 weeks)	257	417	196	376	342	551
Subject 3 (30 weeks)	330	458	208	419	413	730
Subject 4 (35.5 weeks)	589	627	196	321	594	642

AAo: ascending aorta; DA: ductus arteriosus; DAo: descending aorta; Re: Reynolds number

C.2 Mesh-independence Study

The mesh-independence study was conducted based on subject 4. The study started with a $D_{avg}/5$ edge size, where D_{avg} is the average diameter of inflow boundaries, i.e., DAo and DA. Every refinement reduced the edge size by 20%, resulting in a ~50% reduction in mesh cell volume. Figure 8 shows that the $D_{avg}/7.94$ produced mesh-independent results in velocity (less than 3% changes) [54, 55], the metric of interest for this study. Therefore, this mesh was chosen for all simulations, resulting in around 0.25 million tetrahedral cells per mesh.

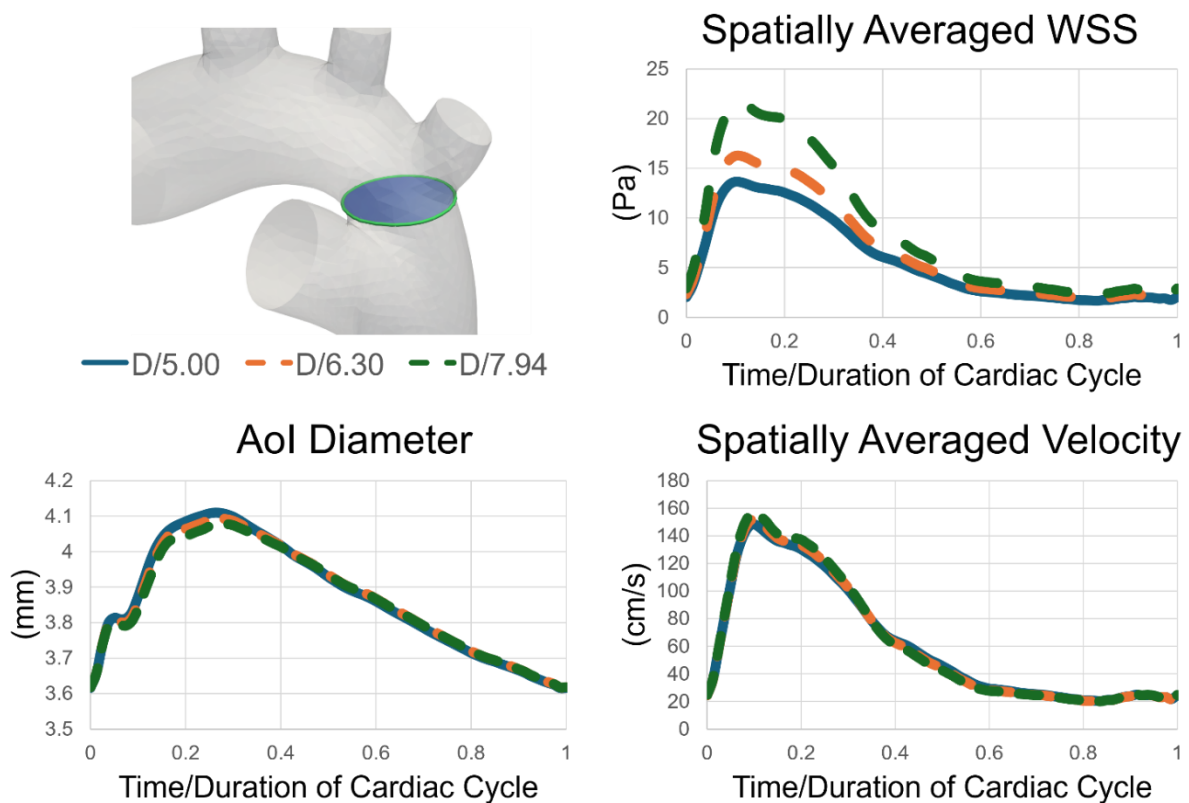


Figure 8. Results of mesh independence study for a representative subject. AoI: aortic isthmus; D: diameter; WSS: wall shear stress.

C.3 Windkessel Parameters for Three Branches

Section B.5 introduces six parameter-splitting algorithms ($m = 2,3,4$ for resistance in equation 6 and $m = 2,3$ for compliance in equation 7). The only approach employed in fetal aortic simulations was the one characterized by $R_i \propto r_i^4$, $C_i \propto r_i^3$ ($m = 4$ for equation 6 and $m = 3$ for equation 7) [24]. However, this study involved a simplified computational model instead of a high-fidelity 3D simulation. Other splitting algorithms have also been widely used in various other studies. Therefore, we explored the differences between the methods characterized by $R_i \propto r_i^4$, $C_i \propto r_i^3$ and by $R_i \propto r_i^2$, $C_i \propto r_i^2$, given that the coefficients of other algorithms lie between these two extremes. Figure 9 illustrates the results, showing that the majority of the variances in pressure and WSS are concentrated on the three branches. The impact of varying the splitting algorithm on the AoI is negligible ($<3\%$). Therefore, we used the $R_i \propto r_i^4$, $C_i \propto r_i^3$ for all simulations in this study.

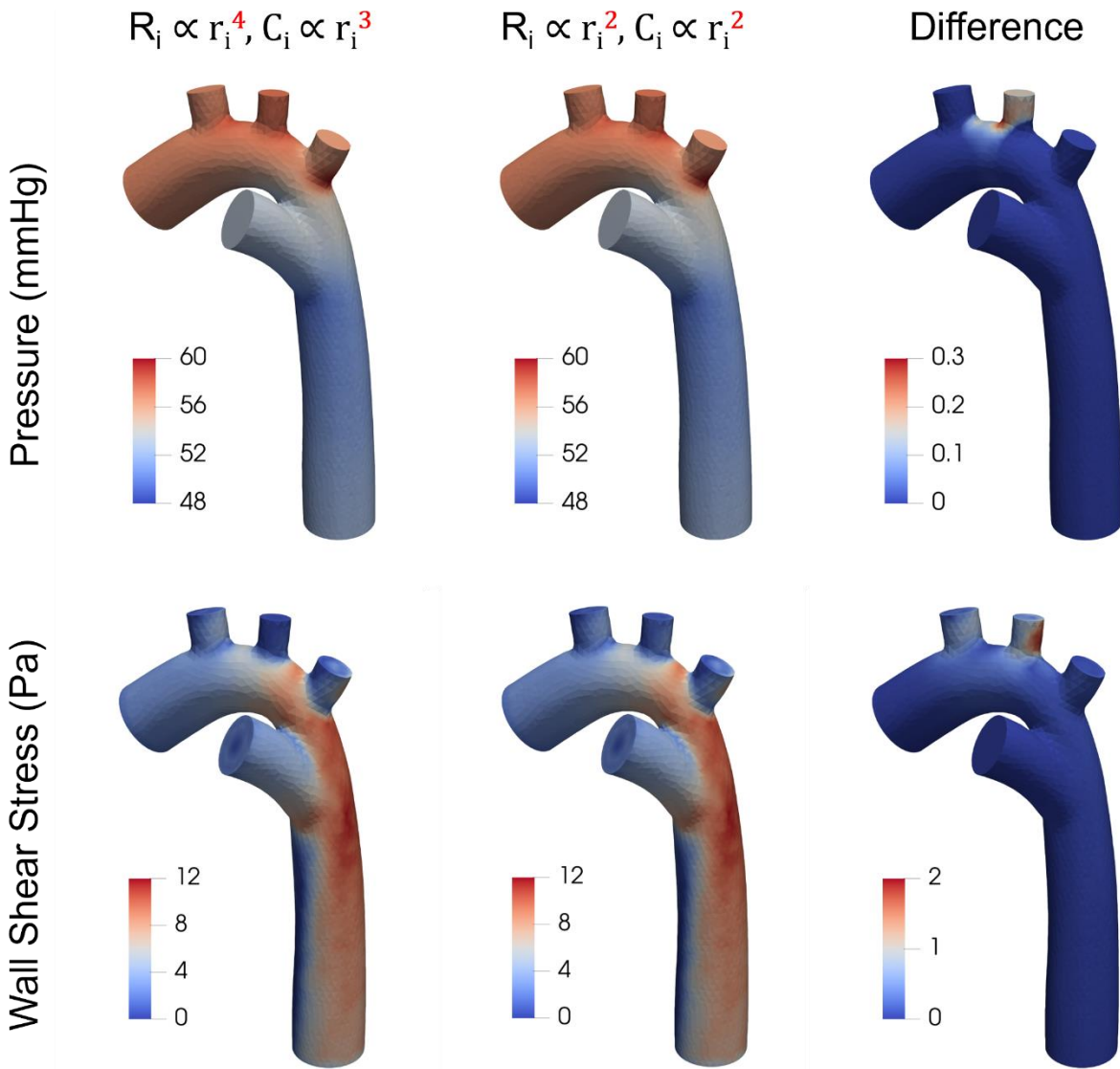


Figure 9. A comparison of parameter-splitting algorithms applied to the three branches for a representative subject. The left column pertains to the method with $m = 4$ for equation 6 and $m = 3$ for equation 7, and the middle column corresponds to the one with $m = 2$ for equation 6 and $m = 2$ for equation 7.

C.4 Convergence of the Iterative Process

Figure 10 illustrates the criteria for stopping the iterative process: (i) the Q_{DAo} from FSI matches the in vivo measured value ($R \geq 0.95$) and (ii) the pulse pressure of DAo (ΔP_{DAo}) from FSI matches the ΔP_{GA} (error $< 5\%$).

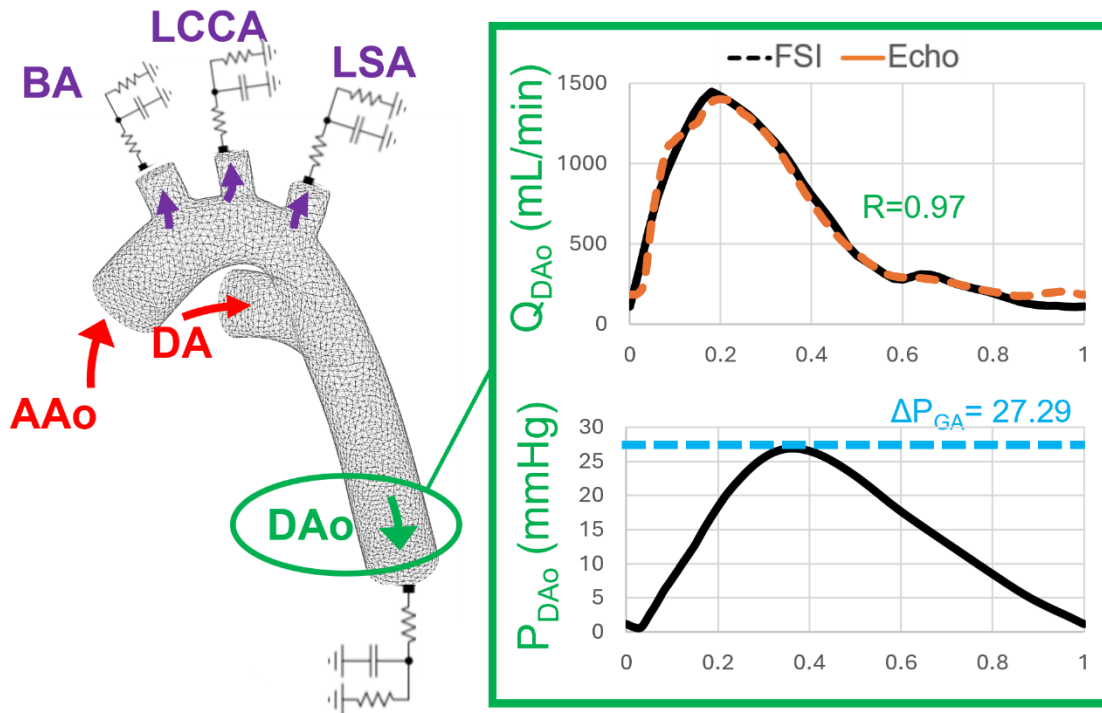


Figure 10. Model verification for a representative subject. AAO: ascending aorta; BA: brachiocephalic artery; descending aorta; DA: ductus arteriosus; DAo: descending aorta; Echo: echocardiography; FSI: fluid-structure interaction; LCCA: left common carotid artery; LSA: left subclavian artery.

It is worth noting that the iterative stage does NOT involve any trial-and-error steps. Therefore, it usually takes three iterations before convergence; an example is shown in Figure 11. The value of ΔP_{DAo_FSI} is usually lower than the anticipated value before the convergence, and $\overline{P_{FSI}}$ could fluctuate between the target values.

Figure 10 also shows that using the pressures from literature, instead of an initial guess of zero, facilitates the convergence of the iterative process. Also, the difference of $\overline{P_{FSI}}$ and ΔP_{DAo_FSI} from the three branches to DAo are 3.2–14.7% and 3.6–41.1% based on the value at the Dao, respectively.

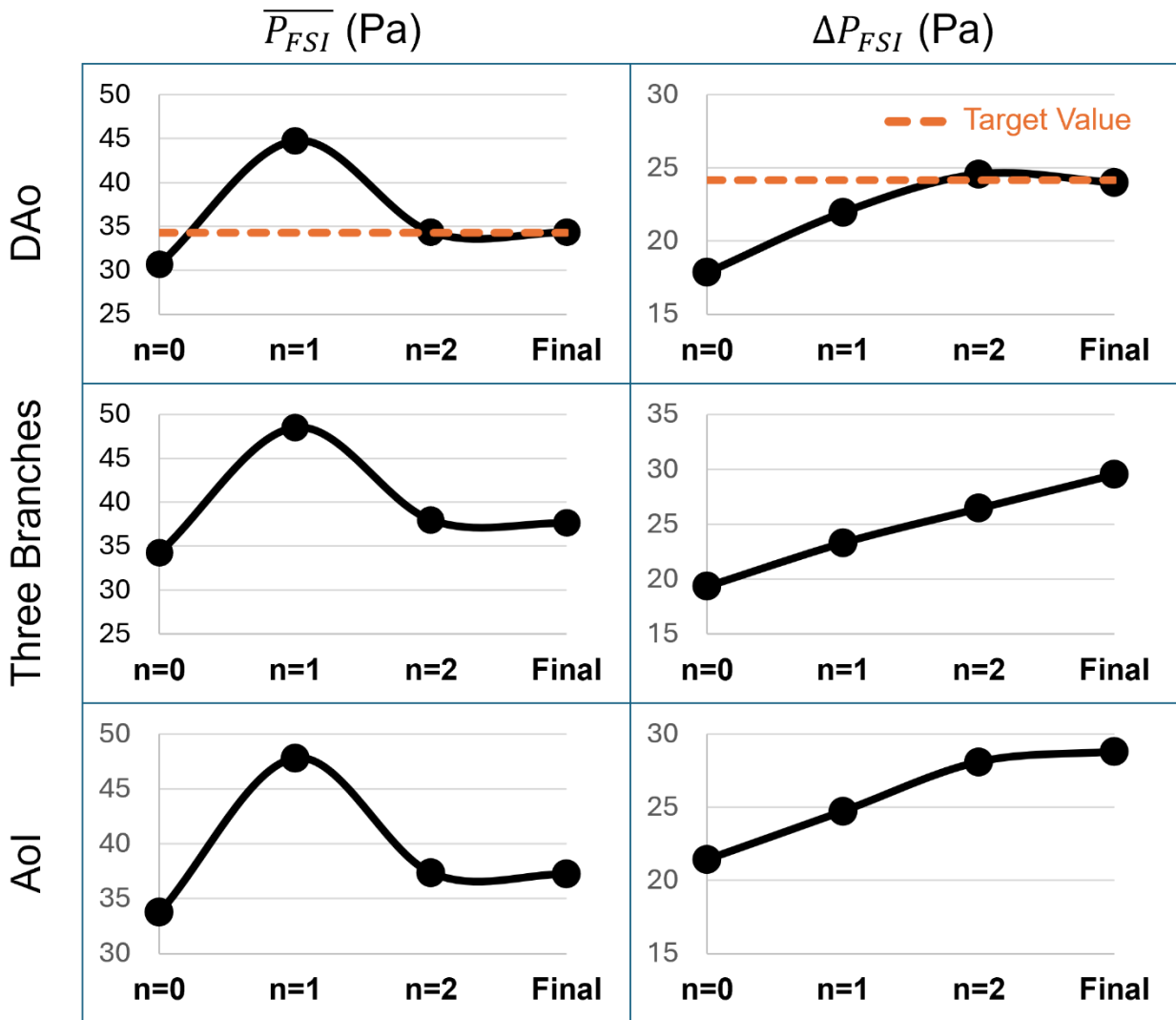


Figure 11. Pressure histories of a representative subject during the iterative stage. Here, $n = 0$ corresponds to step (2) in Figure 5; $n \geq 1$ is linked to step (3) in Figure 5; and “Final” denotes step (5) in Figure 5. AoI: aortic isthmus; DAo: descending aorta; FSI: fluid-structure interaction.

C.5 Validation

The criteria of a successful validation were that (i) the diameter of the AoI matches the in vivo measured value (error < 5%) and (ii) the velocity at AoI reasonably agrees with the in vivo measurement ($R > 0.95$). Figure 12 demonstrates the validation results of the proposed FSI model in four subjects. They all successfully met the two criteria.

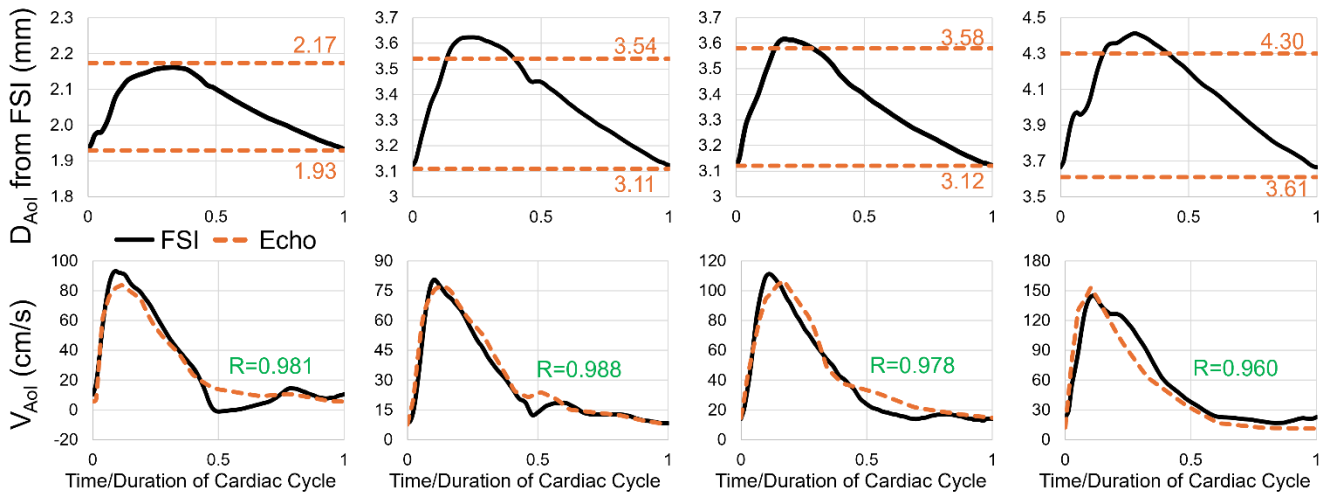


Figure 12. Comparisons for the velocity and diameter at the aortic isthmus for all subjects. D_{AoI} : diameter of the aortic isthmus; Echo: echocardiography; FSI: fluid-structure interaction; V_{AoI} : velocity at the aortic isthmus.

C.6 Biomechanics of Fetal Aorta

Figure 13 illustrates the pressure and particle tracking results for all subjects. The pressure contours explicitly depict the remarkable pressure drop from the AAO to the DAO. The particle line indicates that AAO flow bifurcates into four streams: three of them flow to BA, LCCA, and LSA; the other one merges with the DA flow and exists through the DAO.

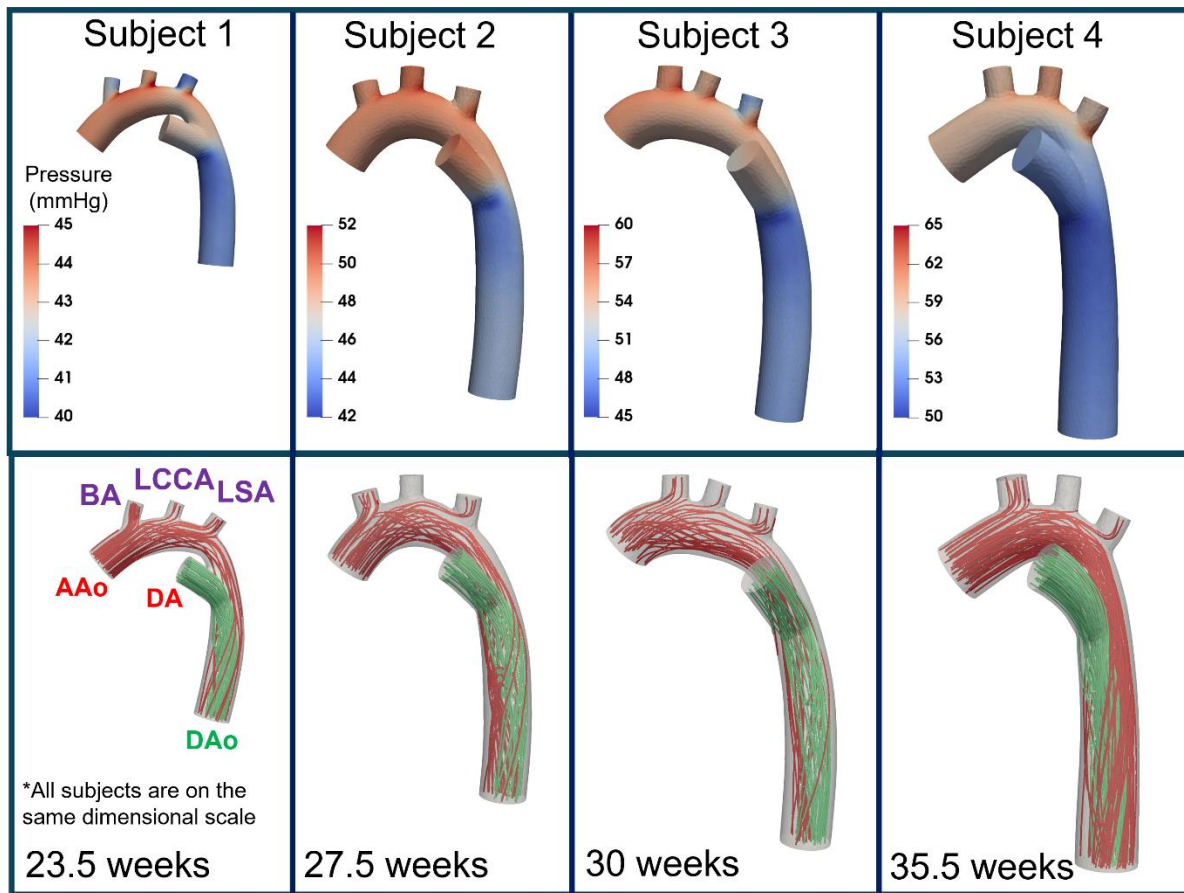


Figure 13. Pressure and particle path (colored by velocity) for all subjects. AAO: ascending aorta; BA: brachiocephalic artery; DA: ductus arteriosus; DAo: descending aorta; LCCA: left common carotid artery; LSA: left subclavian artery.

Table 2 summarizes the material property and diameter changes for all subjects, showing the AoI diameters obtained in good agreement between the FEA and the *in vivo* measurements.

Table 2. Material properties and vessel changes of all subjects.

	Young's Modulus (MPa)	D _{AoI} in mm (min-max)	
		Simulation	in vivo
Subject 1	0.165	1.93-2.16	1.93-2.17
Subject 2	0.185	3.12-3.63	3.11-3.54
Subject 3	0.2	3.12-3.62	3.12-3.58
Subject 4	0.15	3.66-4.41	3.61-4.30

D_{AoI}: diameter of the aortic isthmus; MPa: Megapascal;

D. Discussion

D.1 Patient Selection

This study meticulously chose four fetal aortas that span a broad spectrum of GAs, featuring remarkably diverse geometrical dimensions (illustrated in Figures 6 and 7) and flow conditions (demonstrated in Table 1). Both the geometry and flow increase with GA, with the rate of increase closely aligning with that reported in previous studies [19]. The highest Reynolds number is observed in DAo, as detailed in Table 1. However, no evidence of turbulence was observed because of the relatively low Reynolds numbers across all cases.

D.2 Model Development, Verification, and Validation

The primary difference between the fetal aorta and the pediatric/adult aorta is the presence of the DA. This vessel complicates both the anatomy and FSI modeling of fetal aortas. In addition, the in vivo measurement is limited because the pressure is unavailable for all vessels. Previous articles in the literature only reported the mean and pulse pressure in the DAo. The remarkable pressure drop from the AAo to the DAo, highlighted in Figures 11 and 13, introduces two notable “discontinuities” in developing our workflow:

1. The determination of the fetal aorta’s material properties necessitates knowing the pulse pressure at the AoI, which is considerably higher than that at the DAo by as much as 41.1%.
2. The calculation of the WK parameters for the three branches (BA, LCCA, and LSA) requires both the mean and pulse pressures at the AAo. Whereas the difference in mean pressure is minimal (around 3%) in some subjects, it can reach up to 14% in others.

All these “discontinuities” represent challenges for personalized FSI of the fetal aorta. However, our workflow takes less than three iterations to achieve all verification requirements. Moreover, we conducted the validation in a more rigorous way, because the correlation coefficients (in Figure 12) factor in all errors during a cardiac cycle. Previous studies validated their model concerning single velocity values, e.g., peak systole.

D.3 Hemodynamics in the Fetal Aorta

In addition to the pressure drops across the AoI, the presence of the DA led to flow confluence, as shown in Figure 13. The remainder of the AAo flow through the AoI merges with the DA flow and generates a helical flow. The direction of flow swirling was clockwise downward to the DAo, similar to the flow within the DAo of children

and adults [56, 57]. However, the helical flow observed in this study stems from flow confluence near the DA compared to the flow within children and adults, primarily driven by the twisting motion of heart contraction and aortic valve biomechanics. Nevertheless, the helical flow plays many positive physiological roles, including facilitating blood flow transport, enhancing nutrient transport from the blood to the arterial wall, and reducing the accumulation of atherogenic low-density lipoproteins on the endothelial surface of arteries [57].

Due to the absence of precise flow measurements for the three branches (BA, LSSA, and LCA), we assessed the robustness of applying fluid dynamics theories and clinical insights to flow splitting, as discussed in Section B.5. A specific method ($R_i \propto r_i^4$, $C_i \propto r_i^3$, depicted in Figure 9) has previously been employed in the 3D flow modeling of the fetal aorta. Yet, the influence of various flow-splitting algorithms on the 3D hemodynamic evaluation of the fetal aorta has not been scrutinized. Our findings indicate that the primary effect of these algorithms is observed in the three branches, the impact of which appears to be minimal on their downstream areas, such as at the AoI. However, our investigation was limited to a single fetus. A study involving a larger group of subjects is warranted for a comprehensive understanding, especially if the measurements in the three branches are significant.

D.4 Aortic Stiffness

Ventricular-arterial coupling, a clinically important determinant of cardiovascular performance, measures interactions between the heart and the arterial system [58-61]. The proposed flow model produced great agreements regarding vessel deformation when we compared the AoI diameter obtained by FSI simulation and that obtained by clinical measurement. Our method represents the *first-of-its-kind* approach to estimating the material properties of the fetal aorta, gaining acceptability from prior simulation studies on fetal circulation [12, 13, 62]. Aortic stiffness is a crucial metric in the calculation of ventricular-arterial coupling. However, measuring in vivo aortic stiffness in fetal aortas is challenging, and previous studies adopted simplified estimations. The uncertainty of the stiffness measurements resulted in conflicting trends between the aortic stiffness in fetuses and GA. Some studies demonstrated a decrease in aortic stiffness with GA [23, 39], and others reported an increasing trend [59, 60]. A few recent studies support the decreasing trend using indirect evidence. Miyashita *et al.* revealed a negative relationship between pulse-wave velocity and GA and suggested that pulse-wave velocity was positively correlated with vessel stiffness [61]. Zhong *et al.* reported a decrease in the aortic strain as GA increases, alluding to the fact

that the strain was significantly negatively associated with stiffness [58]. Our inversed method was much more high-fidelity than the simplified theoretical models used in previous studies. Interestingly, the information presented in Table 2 indicates a mixed pattern in aortic stiffness relative to GA: It shows an increase prior to 30 weeks and a decrease thereafter. However, the limited size of the sample makes it necessary to approach the generalization of these findings with caution, suggesting the need for further research.

D.5 Clinical Implications

Computational flow models offer a cost-effective means to analyze blood flow and hemodynamics, providing critical insights into the underlying mechanisms of cardiovascular and cerebrovascular diseases [63-65]. The knowledge and tools developed through these models can be applied to improve both diagnosis and prognosis [66, 67]. Additionally, advancements in model-based diagnostics have opened avenues for commercialization, with several start-up companies receiving FDA approval for clinical applications. The combined market value of these companies is estimated at \$2.4 billion [68]. Moreover, the predictive capabilities of computational models have been utilized to design, test, and optimize medical devices and therapies for cardiovascular and cerebrovascular diseases [69-74], making them valuable tools for preclinical testing that can subsequently guide the design of clinical trials [75-78]. Finally, computational flow models are powerful tools for predicting the efficacy of proposed surgical interventions or medical devices based on pre-operative anatomical models (also known as surgical or treatment planning) [79-83]. This application of advanced CFD analyzes increases confidence in achieving desired surgical outcomes, prevents potential complications, shortens operative times, and minimizes the need for additional procedures [66, 81, 84-86].

In the context of fetal aortic conditions, the FSI model offers a cost-effective solution for obtaining high-fidelity measurements of WSS in fetal circulation - a crucial flow parameter that is challenging to capture using current imaging techniques. WSS plays a pivotal role in vessel dilation, remodeling, and recurrent coarctation in patients with repaired CoA [87-94]. As an innovative flow metric, WSS might distinguish between healthy and coarcted aortas, leading to advancements in the prenatal diagnosis of CoA, which remains one of the most frequently overlooked CHDs [6, 7]. Additionally, the FSI model could be used to assess the feasibility and safety of non-invasive therapeutic strategies for fetal CoA, such as maternal hyperoxygenation [95-97].

E. Limitations

The present study has several limitations. The primary limitation is related to the material model used. The FSI model employed a homogeneous, linear elastic material model with a constant wall thickness. While these simplifications have been commonly used in previous studies of both fetal and adult aortas [19, 25, 37, 38], they do not fully capture the complex mechanical behavior of arterial tissue. Additionally, there is no direct validation of the assumed material properties against *ex vivo* measurements of fetal aortas. Although obtaining such measurements from healthy fetuses presents significant technical and ethical challenges, the good agreement between the simulated FSI results and clinically measured vessel dimensions and flow velocities provides support for the rationale and accuracy of this approach in estimating fetal aortic material properties. Nonetheless, future research should focus on developing more sophisticated material model [98, 99] and validating these models through *ex vivo* measurements where feasible.

The second limitation involves the boundary conditions, which were simplified using Womersley profiles at the inlets and a Windkessel model at the outlets. While this configuration is widely accepted in cardiovascular simulations [100-103], recent studies increasingly recommend using patient-specific velocity profiles that can only be accurately captured using phase-contrast magnetic resonance imaging [54, 104-106]. Despite the difficulties in obtaining such data for fetal circulation, research has shown that patient-specific velocity profiles are essential for accurately assessing localized WSS when compared to idealized profiles [54, 104, 105, 107, 108]. However, since this study does not focus on localized WSS, using idealized profiles could be acceptable. Similarly, due to the difficulties in acquiring patient-specific data for LCCA, LSA, and BA, a Windkessel model was implemented at these boundaries, and the proposed iterative process was used to achieve physiologically realistic flow distributions. As imaging techniques for fetal circulation advance, future studies should explore the effects of different boundary conditions to improve the precision of hemodynamic simulations.

Third, we calculated the flow rate for the three branches using the formula $Q_{3b} = A_{Ao} + DA - Dao$. Although this approach is appropriate for computing average flow rates, it may introduce mass imbalances in instantaneous flow measurements due to residual volumes caused by vessel deformation. However, since instantaneous flow was used only to estimate the RCR values for the branches, and not directly applied to the FSI model, the mass imbalance

has minimal impact. Furthermore, the WK model maintains mass conservation when integrating the RCR values into the FSI simulation.

Fourth, the computational mesh used in this study was designed to ensure mesh-independent results for velocity but not for WSS. Given that velocity was the primary metric of interest, this mesh configuration was deemed sufficient. Nevertheless, future studies focusing on WSS will require a more refined mesh to ensure an accurate assessment of shear stress.

Lastly, this study has a limited sample size. Although this is a constraint, it is acceptable in the context of previous validations, most of which involved even smaller cohorts [37, 109-112]. Future studies should include larger sample sizes to validate the generalizability of the findings.

F. Conclusions

We proposed a novel personalized flow modeling paradigm utilizing FSI, which is time-efficient and capable of simulating high-fidelity hemodynamics of the fetal aorta. To date, this is *the first* paradigm that considers the personalized anatomy, flow, and material properties of the fetal aorta. It provides new evidence of the high-fidelity hemodynamics and biomechanics of the fetal aorta. More importantly, *this paradigm was successfully implemented and rigorously validated against clinically measured dimensions and velocities over a cardiac cycle in four fetuses representing a range of GAs.* Thus, this paradigm represents an important step toward developing a tool to understand the pathogenesis of CHDs related to the fetal aorta and to support clinical applications such as improving diagnosis and prognosis and exploring non-invasive therapeutic strategies for these CHDs.

G. Acknowledgments

We thank the developers and contributors of the following open-source software used in this study, including SimVascular (<https://simvascular.github.io/>) for numerical simulation, RadiAnt DICOM Viewer (<https://www.radiantviewer.com>) for handling DICOM images, and 3D Slicer (<https://www.slicer.org/>) for refining reconstruction. We also extend our gratitude to the members of the Artificial Intelligence and Modeling Laboratory for Cardiovascular Diseases (AIMCardio Lab), including postdoctoral fellows, graduate students, undergraduates, and high school students, for their support in flow segmentation, anatomical reconstruction, method development, and document editing and refinement for this study.

H. Disclosures

All authors declare that they have no conflicts of interest.

References

- [1] J.I. Hoffman, S. Kaplan, The incidence of congenital heart disease, *J Am Coll Cardiol*, 39 (2002) 1890-1900.
- [2] K. Lee, B. Khoshnood, L. Chen, S.N. Wall, W.J. Cromie, R.L. Mittendorf, Infant mortality from congenital malformations in the United States, 1970-1997, *Obstet Gynecol*, 98 (2001) 620-627.
- [3] Q. Yang, H. Chen, A. Correa, O. Devine, T.J. Mathews, M.A. Honein, Racial differences in infant mortality attributable to birth defects in the United States, 1989-2002, *Birth Defects Res A Clin Mol Teratol*, 76 (2006) 706-713.
- [4] E. Beckmann, A.S. Jassar, Coarctation repair-redo challenges in the adults: what to do?, *J Vis Surg*, 4 (2018) 76.
- [5] P. O'Brien, A.C. Marshall, Coarctation of the aorta, *Circulation*, 131 (2015) e363-365.
- [6] E.J. Dijkema, T. Leiner, H.B. Grotenhuis, Diagnosis, imaging and clinical management of aortic coarctation, *Heart*, 103 (2017) 1148-1155.
- [7] J.I. Hoffman, The challenge in diagnosing coarctation of the aorta, *Cardiovasc J Afr*, 29 (2018) 252-255.
- [8] Z.A. Wei, M.A. Fogel, Engineering Perspective on Cardiovascular Simulations of Fontan Hemodynamics: Where Do We Stand with a Look Towards Clinical Application, *Cardiovasc Eng Technol*, 12 (2021) 618-630.
- [9] R. Mittal, J.H. Seo, V. Vedula, Y.J. Choi, H. Liu, H.H. Huang, S. Jain, L. Younes, T. Abraham, R.T. George, Computational modeling of cardiac hemodynamics: Current status and future outlook, *J Comput Phys*, 305 (2016) 1065-1082.
- [10] A.L. Marsden, Optimization in Cardiovascular Modeling, *Annu Rev Fluid Mech*, 46 (2014) 519-546.
- [11] A.L. Marsden, M. Esmaily-Moghadam, Multiscale Modeling of Cardiovascular Flows for Clinical Decision Support, *Appl Mech Rev*, 67 (2015) 1-11.
- [12] H. Wiputra, C.Q. Lai, G.L. Lim, J.J. Heng, L. Guo, S.M. Soomar, H.L. Leo, A. Biwas, C.N. Mattar, C.H. Yap, Fluid mechanics of human fetal right ventricles from image-based computational fluid dynamics using 4D clinical ultrasound scans, *Am J Physiol Heart Circ Physiol*, 311 (2016) H1498-H1508.
- [13] H. Wiputra, C.K. Chen, E. Talbi, G.L. Lim, S.M. Soomar, A. Biswas, C.N.Z. Mattar, D. Bark, H.L. Leo, C.H. Yap, Human fetal hearts with tetralogy of Fallot have altered fluid dynamics and forces, *Am J Physiol Heart Circ Physiol*, 315 (2018) H1649-H1659.
- [14] H.E. Salman, R.Y. Kamal, H.C. Yalcin, Numerical Investigation of the Fetal Left Heart Hemodynamics During Gestational Stages, *Front Physiol*, 12 (2021) 731428.
- [15] M. Malvè, M. Cilla, E. Peña, M.A. Martínez, Impact of the Fluid-Structure Interaction Modeling on the Human Vessel Hemodynamics, *Advances in Biomechanics and Tissue Regeneration 2019*, pp. 79-93.
- [16] M.N. Antonuccio, A. Mariotti, B.M. Fanni, K. Capellini, C. Capelli, E. Sauvage, S. Celi, Effects of Uncertainty of Outlet Boundary Conditions in a Patient-Specific Case of Aortic Coarctation, *Ann Biomed Eng*, 49 (2021) 3494-3507.
- [17] R. Campobasso, F. Condemi, M. Viallon, P. Croisille, S. Campisi, S. Avril, Evaluation of Peak Wall Stress in an Ascending Thoracic Aortic Aneurysm Using FSI Simulations: Effects of Aortic Stiffness and Peripheral Resistance, *Cardiovasc Eng Technol*, 9 (2018) 707-722.
- [18] V. Mendez, M. Di Giuseppe, S. Pasta, Comparison of hemodynamic and structural indices of ascending thoracic aortic aneurysm as predicted by 2-way FSI, CFD rigid wall simulation and patient-specific displacement-based FEA, *Comput Biol Med*, 100 (2018) 221-229.

- [19] M. Nowak, B. Melka, M. Rojczyk, M. Gracka, A.J. Nowak, A. Golda, W.P. Adamczyk, B. Isaac, R.A. Bialecki, Z. Ostrowski, The protocol for using elastic wall model in modeling blood flow within human artery, *European Journal of Mechanics - B/Fluids*, 77 (2019) 273-280.
- [20] P. Reymond, P. Crosetto, S. Deparis, A. Quarteroni, N. Stergiopoulos, Physiological simulation of blood flow in the aorta: comparison of hemodynamic indices as predicted by 3-D FSI, 3-D rigid wall and 1-D models, *Med Eng Phys*, 35 (2013) 784-791.
- [21] A.W. Bowman, *A Practical Guide to Fetal Echocardiography: Normal and Abnormal Hearts*, 2nd ed, American Journal of Roentgenology, 195 (2010) W479-W479.
- [22] X. Zhang, H. Haneishi, H. Liu, Impact of ductus arteriosus constriction and restrictive foramen ovale on global hemodynamics for term fetuses with d-TGA, *Int J Numer Method Biomed Eng*, (2019) e3231.
- [23] P. Garcia-Canadilla, F. Crispi, M. Cruz-Lemini, B. Valenzuela-Alcaraz, P.A. Rudenick, E. Gratacos, B.H. Bijns, Understanding the Aortic Isthmus Doppler Profile and Its Changes with Gestational Age Using a Lumped Model of the Fetal Circulation, *Fetal Diagn Ther*, 41 (2017) 41-50.
- [24] P. Garcia-Canadilla, F. Crispi, M. Cruz-Lemini, S. Triunfo, A. Nadal, B. Valenzuela-Alcaraz, P.A. Rudenick, E. Gratacos, B.H. Bijns, Patient-specific estimates of vascular and placental properties in growth-restricted fetuses based on a model of the fetal circulation, *Placenta*, 36 (2015) 981-989.
- [25] P. Garcia-Canadilla, P.A. Rudenick, F. Crispi, M. Cruz-Lemini, G. Palau, O. Camara, E. Gratacos, B.H. Bijns, A computational model of the fetal circulation to quantify blood redistribution in intrauterine growth restriction, *PLoS Comput Biol*, 10 (2014) e1003667.
- [26] Z. Chen, H. Zhao, Y. Zhao, J. Han, X. Yang, A. Throckmorton, Z. Wei, S. Ge, Y. He, Retrograde flow in aortic isthmus in normal and fetal heart disease by principal component analysis and computational fluid dynamics, *Echocardiography*, 39 (2022) 166-177.
- [27] Z. Chen, H. Zhao, Y. Zhao, J. Han, C. Do-Nguyen, Z.A. Wei, Y. He, S. Ge, Diminished aortic flow in fetus and its implications in development of aortic coarctation and arch interruption: a 3D/4D fetal echocardiography and computational fluid dynamics study, *American Heart Association Scientific Sessions Virtual Meeting*, 2020.
- [28] Z. Chen, H. Zhao, Y. Zhao, C. Do-Nguyen, Z.A. Wei, a.P. Yoganathan, Y. He, S. Ge, Diminished flow in aorta by 3D/4D fetal echocardiography and computational fluid dynamics: implications in coarctation, *International Society of Ultrasound in Obstetrics & Gynecology Virtual Meeting*, 2020.
- [29] E. Tang, Z.A. Wei, M.A. Fogel, A. Veneziani, A.P. Yoganathan, Fluid-Structure Interaction Simulation of an Intra-Atrial Fontan Connection, *Biology (Basel)*, 9 (2020).
- [30] A. Updegrave, N.M. Wilson, J. Merkow, H. Lan, A.L. Marsden, S.C. Shadden, SimVascular: An Open Source Pipeline for Cardiovascular Simulation, *Ann Biomed Eng*, 45 (2017) 525-541.
- [31] K. Nicolaides, G. Rizzo, K. Hecher, R. Ximenes, *Doppler in obstetrics*, (2005).
- [32] K. Hecher, S. Campbell, P. Doyle, K. Harrington, K. Nicolaides, Assessment of fetal compromise by Doppler ultrasound investigation of the fetal circulation. Arterial, intracardiac, and venous blood flow velocity studies, *Circulation*, 91 (1995) 129-138.
- [33] M.A. Quinones, C.M. Otto, M. Stoddard, A. Waggoner, W.A. Zoghbi, N. Doppler Quantification Task Force of the, E. Standards Committee of the American Society of, Recommendations for quantification of Doppler echocardiography: a report from the Doppler Quantification Task Force of the Nomenclature and Standards Committee of the American Society of Echocardiography, *J Am Soc Echocardiogr*, 15 (2002) 167-184.
- [34] M. Tree, Z.A. Wei, B. Munz, K. Maher, S. Deshpande, T. Slesnick, A. Yoganathan, A Method for In Vitro TCPC Compliance Verification, *J Biomech Eng-T Asme*, 139 (2017) 064502-064502.
- [35] M.-C. Hsu, Y. Bazilevs, Blood vessel tissue prestress modeling for vascular fluid-structure interaction simulation, *Finite Elements in Analysis and Design*, 47 (2011) 593-599.

- [36] K. Baumler, V. Vedula, A.M. Sailer, J. Seo, P. Chiu, G. Mistelbauer, F.P. Chan, M.P. Fischbein, A.L. Marsden, D. Fleischmann, Fluid-structure interaction simulations of patient-specific aortic dissection, *Biomech Model Mechanobiol*, 19 (2020) 1607-1628.
- [37] J. Lantz, J. Renner, M. Karlsson, Wall Shear Stress in a Subject Specific Human Aorta — Influence of Fluid-Structure Interaction, *International Journal of Applied Mechanics*, 03 (2012) 759-778.
- [38] J.P. van den Wijngaard, B.E. Westerhof, D.J. Faber, M.M. Ramsay, N. Westerhof, M.J. van Gemert, Abnormal arterial flows by a distributed model of the fetal circulation, *Am J Physiol Regul Integr Comp Physiol*, 291 (2006) R1222-1233.
- [39] P.C. Struijk, V.J. Mathews, T. Loupas, P.A. Stewart, E.B. Clark, E.A. Steegers, J.W. Wladimiroff, Blood pressure estimation in the human fetal descending aorta, *Ultrasound Obstet Gynecol*, 32 (2008) 673-681.
- [40] C.A. Figueroa, I.E. Vignon-Clementel, K.E. Jansen, T.J.R. Hughes, C.A. Taylor, A coupled momentum method for modeling blood flow in three-dimensional deformable arteries, *Computer Methods in Applied Mechanics and Engineering*, 195 (2006) 5685-5706.
- [41] M. Esmaily Moghadam, I.E. Vignon-Clementel, R. Figliola, A.L. Marsden, A modular numerical method for implicit 0D/3D coupling in cardiovascular finite element simulations, *J Comput Phys*, 244 (2013) 63-79.
- [42] P.C. Africa, I. Fumagalli, M. Bucelli, A. Zingaro, M. Fedele, L. Dede, A. Quarteroni, lifex-cfd: An open-source computational fluid dynamics solver for cardiovascular applications, *Comput Phys Commun*, 296 (2024).
- [43] M. Esmaily Moghadam, Y. Bazilevs, T.-Y. Hsia, I.E. Vignon-Clementel, A.L. Marsden, A comparison of outlet boundary treatments for prevention of backflow divergence with relevance to blood flow simulations, *Computational Mechanics*, 48 (2011) 277-291.
- [44] C.A. Taylor, K. Petersen, N. Xiao, M. Sinclair, Y. Bai, S.R. Lynch, A. UpdePac, M. Schaap, Patient-specific modeling of blood flow in the coronary arteries, *Computer Methods in Applied Mechanics and Engineering*, 417 (2023).
- [45] W.K. Laskey, H.G. Parker, V.A. Ferrari, W.G. Kussmaul, A. Noordergraaf, Estimation of total systemic arterial compliance in humans, *J Appl Physiol* (1985), 69 (1990) 112-119.
- [46] H.J. Kim, I.E. Vignon-Clementel, C.A. Figueroa, K.E. Jansen, C.A. Taylor, Developing computational methods for three-dimensional finite element simulations of coronary blood flow, *Finite Elements in Analysis and Design*, 46 (2010) 514-525.
- [47] H.J. Kim, I.E. Vignon-Clementel, J.S. Coogan, C.A. Figueroa, K.E. Jansen, C.A. Taylor, Patient-specific modeling of blood flow and pressure in human coronary arteries, *Ann Biomed Eng*, 38 (2010) 3195-3209.
- [48] H.J. Kim, I.E. Vignon-Clementel, C.A. Figueroa, J.F. LaDisa, K.E. Jansen, J.A. Feinstein, C.A. Taylor, On coupling a lumped parameter heart model and a three-dimensional finite element aorta model, *Ann Biomed Eng*, 37 (2009) 2153-2169.
- [49] E. Fevola, F. Ballarin, L. Jimenez-Juan, S. Fremes, S. Grivet-Talocia, G. Rozza, P. Triverio, An optimal control approach to determine resistance-type boundary conditions from in-vivo data for cardiovascular simulations, *Int J Numer Method Biomed Eng*, 37 (2021) e3516.
- [50] C. Chnafa, P. Bouillot, O. Brina, B.M.A. Delattre, M.I. Vargas, K.O. Lovblad, V.M. Pereira, D.A. Steinman, Vessel calibre and flow splitting relationships at the internal carotid artery terminal bifurcation, *Physiol Meas*, 38 (2017) 2044-2057.
- [51] M. Zamir, P. Sinclair, T.H. Wonnacott, Relation between diameter and flow in major branches of the arch of the aorta, *J Biomech*, 25 (1992) 1303-1310.
- [52] C.D. Murray, The Physiological Principle of Minimum Work: II Oxygen Exchange in Capillaries, *Proceedings of the National Academy of Sciences*, 12 (1926) 299-304.
- [53] C.D. Murray, The Physiological Principle of Minimum Work: I The Vascular System and the Cost of Blood Volume, *Proceedings of the National Academy of Sciences*, 12 (1926) 207-214.

- [54] Z.A. Wei, C. Huddleston, P.M. Trusty, S. Singh-Gryzbon, M.A. Fogel, A. Veneziani, A.P. Yoganathan, Analysis of Inlet Velocity Profiles in Numerical Assessment of Fontan Hemodynamics, *Ann Biomed Eng*, 47 (2019) 2258-2270.
- [55] Z.A. Wei, M. Tree, P.M. Trusty, W. Wu, S. Singh-Gryzbon, A. Yoganathan, The Advantages of Viscous Dissipation Rate over Simplified Power Loss as a Fontan Hemodynamic Metric, *Ann Biomed Eng*, 46 (2018) 404-416.
- [56] P.J. Kilner, G.Z. Yang, R.H. Mohiaddin, D.N. Firmin, D.B. Longmore, Helical and retrograde secondary flow patterns in the aortic arch studied by three-directional magnetic resonance velocity mapping, *Circulation*, 88 (1993) 2235-2247.
- [57] X. Liu, A. Sun, Y. Fan, X. Deng, Physiological significance of helical flow in the arterial system and its potential clinical applications, *Ann Biomed Eng*, 43 (2015) 3-15.
- [58] X. Zhong, Y. Luo, D. Zhou, M. Liu, J. Zhou, R. Xu, S. Zeng, Maturation Fetus Ascending Aorta Elastic Properties: Circumferential Strain and Longitudinal Strain by Velocity Vector Imaging, *Front Cardiovasc Med*, 9 (2022) 840494.
- [59] M. Akira, S. Yoshiyuki, Placental circulation, fetal growth, and stiffness of the abdominal aorta in newborn infants, *J Pediatr-Ur*, 148 (2006) 49-53.
- [60] M. Taketazu, M. Sugimoto, H. Saiki, H. Ishido, S. Masutani, H. Senzaki, Developmental Changes in Aortic Mechanical Properties in Normal Fetuses and Fetuses with Cardiovascular Disease, *Pediatr Neonatol*, 58 (2017) 245-250.
- [61] S. Miyashita, J. Muromoto, J. Muromoto, K. Ozawa, N. Yaegashi, H. Hasegawa, H. Kanai, Measurement of internal diameter changes and pulse wave velocity in fetal descending aorta using the ultrasonic phased-tracking method in normal and growth-restricted fetuses, *Ultrasound Med Biol*, 41 (2015) 1311-1319.
- [62] H.E. Salman, H.C. Yalcin, Computational Modeling of Blood Flow Hemodynamics for Biomechanical Investigation of Cardiac Development and Disease, *J Cardiovasc Dev Dis*, 8 (2021).
- [63] S. Singh-Gryzbon, V. Sadri, M. Toma, E.L. Pierce, Z.A. Wei, A.P. Yoganathan, Development of a Computational Method for Simulating Tricuspid Valve Dynamics, *Ann Biomed Eng*, 47 (2019) 1422-1434.
- [64] S. Singh-Gryzbon, B. Ncho, V. Sadri, S.S. Bhat, S.S. Kollapaneni, D. Balakumar, Z.A. Wei, P. Ruile, F.J. Neumann, P. Blanke, A.P. Yoganathan, Influence of Patient-Specific Characteristics on Transcatheter Heart Valve Neo-Sinus Flow: An In Silico Study, *Ann Biomed Eng*, 48 (2020) 2400-2411.
- [65] M. Toma, S. Singh-Gryzbon, E. Frankini, Z.A. Wei, A.P. Yoganathan, Clinical Impact of Computational Heart Valve Models, *Materials (Basel)*, 15 (2022).
- [66] C. Chiastra, M. Zuin, G. Rigatelli, F. D'Ascenzo, G.M. De Ferrari, C. Collet, Y.S. Chatzizisis, D. Gallo, U. Morbiducci, Computational fluid dynamics as supporting technology for coronary artery disease diagnosis and treatment: an international survey, *Front Cardiovasc Med*, 10 (2023) 1216796.
- [67] P.D. Morris, A. Narracott, H. von Tengg-Kobligk, D.A. Silva Soto, S. Hsiao, A. Lungu, P. Evans, N.W. Bressloff, P.V. Lawford, D.R. Hose, J.P. Gunn, Computational fluid dynamics modelling in cardiovascular medicine, *Heart*, 102 (2016) 18-28.
- [68] HeartFlow announces plans to merge, go public in deal worth \$2.4B, 2021.
- [69] B.M. Yun, J. Wu, H.A. Simon, S. Arjunon, F. Sotiropoulos, C.K. Aidun, A.P. Yoganathan, A numerical investigation of blood damage in the hinge area of aortic bileaflet mechanical heart valves during the leakage phase, *Ann Biomed Eng*, 40 (2012) 1468-1485.
- [70] B. Min Yun, C.K. Aidun, A.P. Yoganathan, Blood damage through a bileaflet mechanical heart valve: a quantitative computational study using a multiscale suspension flow solver, *J Biomech Eng-T Asme*, 136 (2014) 101009.

- [71] D.D. Soerensen, K. Pekkan, D. de Zelicourt, S. Sharma, K. Kanter, M. Fogel, A.P. Yoganathan, Introduction of a new optimized total cavopulmonary connection, *Ann Thorac Surg*, 83 (2007) 2182-2190.
- [72] Z.A. Wei, K. Ratnayaka, B. Si, S. Singh-Gryzbon, M.A. Cetatou, M.A. Fogel, T. Slesnick, A.P. Yoganathan, J.J. Nigro, An Anterior Anastomosis for the Modified Fontan Connection: A Hemodynamic Analysis, *Semin Thorac Cardiovasc Surg*, 33 (2021) 816-823.
- [73] P.M. Trusty, Z. Wei, M. Sales, K.R. Kanter, M.A. Fogel, A.P. Yoganathan, T.C. Slesnick, Y-graft modification to the Fontan procedure: Increasingly balanced flow over time, *J Thorac Cardiovasc Surg*, 159 (2020) 652-661.
- [74] K. Kohli, Z.A. Wei, V. Sadri, A.W. Siefert, P. Blanke, E. Perdoncin, A.B. Greenbaum, J.M. Khan, R.J. Lederman, V.C. Babaliaros, A.P. Yoganathan, J.N. Oshinski, Assessing the Hemodynamic Impact of Anterior Leaflet Laceration in Transcatheter Mitral Valve Replacement: An in silico Study, *Front Cardiovasc Med*, 9 (2022) 869259.
- [75] M. Viceconti, F. Pappalardo, B. Rodriguez, M. Horner, J. Bischoff, F. Musuamba Tshinanu, In silico trials: Verification, validation and uncertainty quantification of predictive models used in the regulatory evaluation of biomedical products, *Methods*, 185 (2021) 120-127.
- [76] A. Sarrami-Foroushani, T. Lassila, M. MacRaid, J. Asquith, K.C.B. Roes, J.V. Byrne, A.F. Frangi, In-silico trial of intracranial flow diverters replicates and expands insights from conventional clinical trials, *Nat Commun*, 12 (2021) 3861.
- [77] C. Miller, R.M. Padmos, M. van der Kolk, T.I. Jozsa, N. Samuels, Y. Xue, S.J. Payne, A.G. Hoekstra, In silico trials for treatment of acute ischemic stroke: Design and implementation, *Comput Biol Med*, 137 (2021) 104802.
- [78] M. Viceconti, A. Henney, E. Morley-Fletcher, In silico clinical trials: how computer simulation will transform the biomedical industry, *International Journal of Clinical Trials*, 3 (2016).
- [79] P.M. Trusty, Z.A. Wei, T.C. Slesnick, K.R. Kanter, T.L. Spray, M.A. Fogel, A.P. Yoganathan, The first cohort of prospective Fontan surgical planning patients with follow-up data: How accurate is surgical planning?, *J Thorac Cardiovasc Surg*, 157 (2019) 1146-1155.
- [80] P.M. Trusty, T.C. Slesnick, Z.A. Wei, J. Rossignac, K.R. Kanter, M.A. Fogel, A.P. Yoganathan, Fontan Surgical Planning: Previous Accomplishments, Current Challenges, and Future Directions, *J Cardiovasc Transl Res*, 11 (2018) 133-144.
- [81] K. Kohli, Z.A. Wei, V. Sadri, T.F. Easley, E.L. Pierce, Y.N. Zhang, D.D. Wang, A.B. Greenbaum, J.C. Lisko, J.M. Khan, R.J. Lederman, P. Blanke, J.N. Oshinski, V. Babaliaros, A.P. Yoganathan, Framework for Planning TMVR using 3-D Imaging, In Silico Modeling, and Virtual Reality, *Structural Heart*, 4 (2020) 336-341.
- [82] K. Kohli, Z.A. Wei, A.P. Yoganathan, J.N. Oshinski, J. Leipsic, P. Blanke, Transcatheter Mitral Valve Planning and the Neo-LVOT: Utilization of Virtual Simulation Models and 3D Printing, *Curr Treat Options Cardiovasc Med*, 20 (2018) 99.
- [83] E. Garven, A. Throckmorton, Invited commentary: Personalized surgical planning by computational and visual methods in 21st-century medical engineering, *J Card Surg*, 35 (2020) 526-527.
- [84] J. Rossignac, H. Pekkan, B. Whited, K. Kanter, S. Sharma, A. Yoganathan, Surgem: Interactive patient-specific anatomy-editor for hemodynamics analysis and surgery planning, *Technology*, (2007) 1-11.
- [85] A.L. Marsden, Simulation based planning of surgical interventions in pediatric cardiology, *Phys Fluids* (1994), 25 (2013) 101303.
- [86] A.S. Rao, P.G. Menon, Presurgical planning using image-based in silico anatomical and functional characterization of Tetralogy of Fallot with associated anomalies, *Interact Cardiovasc Thorac Surg*, 20 (2015) 149-156.

- [87] M.O. Khan, J.S. Tran, H. Zhu, J. Boyd, R.R.S. Packard, R.P. Karlsberg, A.M. Kahn, A.L. Marsden, Low Wall Shear Stress Is Associated with Saphenous Vein Graft Stenosis in Patients with Coronary Artery Bypass Grafting, *J Cardiovasc Transl Res*, 14 (2021) 770-781.
- [88] B. Zhang, J. Gu, M. Qian, L. Niu, H. Zhou, D. Ghista, Correlation between quantitative analysis of wall shear stress and intima-media thickness in atherosclerosis development in carotid arteries, *Biomed Eng Online*, 16 (2017) 137.
- [89] L. Boussel, V. Rayz, C. McCulloch, A. Martin, G. Acevedo-Bolton, M. Lawton, R. Higashida, W.S. Smith, W.L. Young, D. Saloner, Aneurysm growth occurs at region of low wall shear stress: patient-specific correlation of hemodynamics and growth in a longitudinal study, *Stroke*, 39 (2008) 2997-3002.
- [90] A.M. Malek, S.L. Alper, S. Izumo, Hemodynamic shear stress and its role in atherosclerosis, *JAMA*, 282 (1999) 2035-2042.
- [91] J.F. Juffermans, I. Nederend, P.J. van den Boogaard, A.D.J. Ten Harkel, M.G. Hazekamp, H.J. Lamb, A.A.W. Roest, J.J.M. Westenberg, The effects of age at correction of aortic coarctation and recurrent obstruction on adolescent patients: MRI evaluation of wall shear stress and pulse wave velocity, *Eur Radiol Exp*, 3 (2019) 24.
- [92] J.F. LaDisa, Jr., S. Bozdog, J. Olson, R. Ramchandran, J.R. Kersten, T.J. Eddinger, Gene Expression in Experimental Aortic Coarctation and Repair: Candidate Genes for Therapeutic Intervention?, *PLoS One*, 10 (2015) e0133356.
- [93] J.F. LaDisa, Jr., C. Alberto Figueroa, I.E. Vignon-Clementel, H.J. Kim, N. Xiao, L.M. Ellwein, F.P. Chan, J.A. Feinstein, C.A. Taylor, Computational simulations for aortic coarctation: representative results from a sampling of patients, *J Biomech Eng-T Asme*, 133 (2011) 091008.
- [94] L. Ait Ali, N. Martini, C. Grigoratos, D. Della Latta, D. Chiappino, P. Festa, 4-Dimensional Velocity Mapping Cardiac Magnetic Resonance of Extracardiac Bypass for Aortic Coarctation Repair, *JACC Case Rep*, 1 (2019) 17-20.
- [95] L.A. Edwards, D.A. Lara, M. Sanz Cortes, J.V. Hunter, S. Andreas, M.J. Nguyen, L.J. Schoppe, J. Zhang, E.M. Smith, S.A. Maskatia, S.K. Sexson-Tejtel, K.N. Lopez, E.J. Lawrence, Y. Wang, M. Challman, N.A. Ayres, C.A. Altman, K. Aagaard, J.A. Becker, S.A. Morris, Chronic Maternal Hyperoxygenation and Effect on Cerebral and Placental Vasoregulation and Neurodevelopment in Fetuses with Left Heart Hypoplasia, *Fetal Diagn Ther*, 46 (2019) 45-57.
- [96] A.M. Rudolph, Maternal hyperoxygenation for the human fetus: should studies be curtailed?, *Pediatr Res*, 87 (2020) 630-633.
- [97] S.L. Lee FT, van Amerom J, Freud L, Jaeggi E, Marini D, Saito M, Szabo A, Milligan N, Saini A, Van Mieghem T, Kingdom J, Miller S, Seed M., The Feasibility and Safety of Maternal Hyperoxygenation in Single Ventricle Congenital Heart Disease: Preliminary Findings., *CNPRM*, (2021).
- [98] M. Liu, L. Liang, W. Sun, Estimation of in vivo constitutive parameters of the aortic wall using a machine learning approach, *Comput Methods Appl Mech Eng*, 347 (2019) 201-217.
- [99] M. Liu, L. Liang, W. Sun, A new inverse method for estimation of in vivo mechanical properties of the aortic wall, *J Mech Behav Biomed Mater*, 72 (2017) 148-158.
- [100] V. Filonova, C.J. Arthurs, I.E. Vignon-Clementel, C.A. Figueroa, Verification of the coupled-momentum method with Womersley's Deformable Wall analytical solution, *Int J Numer Method Biomed Eng*, 36 (2020) e3266.
- [101] A. Quarteroni, A. Veneziani, C. Vergara, Geometric multiscale modeling of the cardiovascular system, between theory and practice, *Computer Methods in Applied Mechanics and Engineering*, 302 (2016) 193-252.
- [102] J. Flores, J. Alastruey, E. Corvera Poire, A Novel Analytical Approach to Pulsatile Blood Flow in the Arterial Network, *Ann Biomed Eng*, 44 (2016) 3047-3068.

- [103] B.M. Yun, L.P. Dasi, C.K. Aidun, A.P. Yoganathan, Computational modelling of flow through prosthetic heart valves using the entropic lattice-Boltzmann method, *J Fluid Mech*, 743 (2014) 170-201.
- [104] U. Morbiducci, R. Ponzini, D. Gallo, C. Bignardi, G. Rizzo, Inflow boundary conditions for image-based computational hemodynamics: impact of idealized versus measured velocity profiles in the human aorta, *J Biomech*, 46 (2013) 102-109.
- [105] D. Hardman, S.I. Semple, J.M. Richards, P.R. Hoskins, Comparison of patient-specific inlet boundary conditions in the numerical modelling of blood flow in abdominal aortic aneurysm disease, *Int J Numer Method Biomed Eng*, 29 (2013) 165-178.
- [106] P. Youssefi, A. Gomez, C. Arthurs, R. Sharma, M. Jahangiri, C. Alberto Figueroa, Impact of Patient-Specific Inflow Velocity Profile on Hemodynamics of the Thoracic Aorta, *J Biomech Eng-T Asme*, 140 (2018) 1-14.
- [107] C. Vergara, R. Ponzini, A. Veneziani, A. Redaelli, D. Neglia, O. Parodi, Womersley number-based estimation of flow rate with Doppler ultrasound: sensitivity analysis and first clinical application, *Comput Methods Programs Biomed*, 98 (2010) 151-160.
- [108] R. Ponzini, C. Vergara, G. Rizzo, A. Veneziani, A. Roghi, A. Vanzulli, O. Parodi, A. Redaelli, Womersley number-based estimates of blood flow rate in Doppler analysis: in vivo validation by means of phase-contrast MRI, *IEEE Trans Biomed Eng*, 57 (2010) 1807-1815.
- [109] W. Yang, F.P. Chan, V.M. Reddy, A.L. Marsden, J.A. Feinstein, Flow simulations and validation for the first cohort of patients undergoing the Y-graft Fontan procedure, *J Thorac Cardiovasc Sur*, 149 (2015) 247-255.
- [110] W. Mao, K. Li, W. Sun, Fluid-Structure Interaction Study of Transcatheter Aortic Valve Dynamics Using Smoothed Particle Hydrodynamics, *Cardiovasc Eng Technol*, 7 (2016) 374-388.
- [111] L. Swanson, B. Owen, A. Keshmiri, A. Deyranlou, T. Aldersley, J. Lawrenson, P. Human, R. De Decker, B. Fourie, G. Comitis, M.E. Engel, B. Keavney, L. Zuhlke, M. Ngoepe, A. Revell, A Patient-Specific CFD Pipeline Using Doppler Echocardiography for Application in Coarctation of the Aorta in a Limited Resource Clinical Context, *Front Bioeng Biotechnol*, 8 (2020) 409.
- [112] J. Sotelo, J. Urbina, I. Valverde, C. Tejos, P. Irarrazaval, M.E. Andia, S. Uribe, D.E. Hurtado, 3D Quantification of Wall Shear Stress and Oscillatory Shear Index Using a Finite-Element Method in 3D CINE PC-MRI Data of the Thoracic Aorta, *IEEE Trans Med Imaging*, 35 (2016) 1475-1487.